Neutral *B*-meson mixing from unquenched lattice QCD with domain-wall light quarks and static *b* quarks

C. Albertus,[1,*] Y. Aoki,[2] P. A. Boyle,[3] N. H. Christ,[4] T. T. Dumitrescu,[4,†] J. M. Flynn,[1] T. Ishikawa,[2,‡] T. Izubuchi,[2,5]
O. Loktik,[4] C. T. Sachrajda,[1] A. Soni,[5] R. S. Van de Water,[5] J. Wennekers,[3,§,‖] and O. Witzel[5]

(RBC and UKQCD Collaborations)

[1]*School of Physics and Astronomy, University of Southampton, Southampton SO17 1BJ, United Kingdom*
[2]*RIKEN-BNL Research Center, Brookhaven National Laboratory, Upton, New York 11973, USA*
[3]*SUPA, School of Physics, The University of Edinburgh, Edinburgh EH9 3JZ, United Kingdom*
[4]*Physics Department, Columbia University, New York, New York 10027, USA*
[5]*Physics Department, Brookhaven National Laboratory, Upton, New York 11973, USA*

We demonstrate a method for calculating the neutral *B*-meson decay constants and mixing matrix elements in unquenched lattice QCD with domain-wall light quarks and static *b*-quarks. Our computation is performed on the "2 + 1" flavor gauge configurations generated by the RBC and UKQCD Collaborations with a lattice spacing of $a \approx 0.11$ fm ($a^{-1} = 1.729$ GeV) and a lattice spatial volume of approximately $(1.8 \text{ fm})^3$. We simulate at three different light sea quark masses with pion masses down to approximately 430 MeV, and extrapolate to the physical quark masses using a phenomenologically-motivated fit function based on next-to-leading order heavy-light meson SU(2) chiral perturbation theory. For the *b*-quarks, we use an improved formulation of the Eichten-Hill action with static link-smearing to increase the signal-to-noise ratio. We also improve the heavy-light axial current used to compute the *B*-meson decay constant to $\mathcal{O}(\alpha_s p a)$ using one-loop lattice perturbation theory. We present initial results for the SU(3)-breaking ratios f_{B_s}/f_{B_d} and $\xi = f_{B_s}\sqrt{B_{B_s}}/f_{B_d}\sqrt{B_{B_d}}$, thereby demonstrating the viability of the method. For the ratio of decay constants, we find $f_{B_s}/f_{B_d} = 1.15(12)$ and for the ratio of mixing matrix elements, we find $\xi = 1.13(12)$, where in both cases the errors reflect the combined statistical and systematic uncertainties, including an estimate of the size of neglected $\mathcal{O}(1/m_b)$ effects.

I. INTRODUCTION

Neutral *B*-meson mixing is a sensitive probe of quark flavor-changing interactions. When combined with experimental measurements of the B_d^0 and B_s^0 oscillation frequencies, precise QCD determinations of the B_d^0 and B_s^0-mixing hadronic matrix elements allow clean determinations of the Cabibbo-Kobayashi-Maskawa (CKM) [1,2] matrix elements $|V_{td}|$ and $|V_{ts}|$ with all sources of systematic uncertainty under control. In the standard model, the mass-difference of the neutral *B*-meson mass eigenstates Δm_q (often called the oscillation frequency) is given by [3,4]

$$\Delta m_q = \frac{G_F^2 m_W^2}{16\pi^2 m_{B_q}} |V_{tq}^* V_{tb}|^2 S_0(x_t)\eta_B \mathcal{M}_q, \qquad (1)$$

where $q \in \{d, s\}$. Both the Inami–Lim function $S_0(x_t)$ with $x_t = m_t^2/m_W^2$ [5] and the QCD coefficient η_B can be computed in perturbation theory [3]. The hadronic contribution to the $\Delta B = 2$ mixing matrix element,

$$\mathcal{M}_q = \langle \bar{B}_q^0 | [\bar{b}\gamma^\mu(1 - \gamma_5)q][\bar{b}\gamma_\mu(1 - \gamma_5)q] | B_q^0 \rangle, \quad (2)$$

must be calculated nonperturbatively from first principles using lattice QCD.

The hadronic matrix element $\mathcal{M}_q$ is conventionally parametrized as

$$\mathcal{M}_q = \tfrac{8}{3} m_{B_q}^2 f_{B_q}^2 B_{B_q}, \qquad (3)$$

where m_{B_q} is the mass of the *B*-meson, f_{B_q} is the *B*-meson decay constant, and B_{B_q} is the *B*-meson bag parameter. Many statistical and systematic uncertainties from lattice calculations cancel in the SU(3)-breaking ratio $\mathcal{M}_s/\mathcal{M}_d$, which would be one in the limit $m_d \to m_s$. It is therefore convenient and conventional to introduce the quantity

*Present address: Departamento de Física Fundamental, Facultad de Ciencias, Universidad de Salamanca, Plaza de la Merced s/n, 37008, Salamanca, Spain.
†Present address: Department of Physics, Princeton University, Princeton, NJ 08544, USA.
‡Present address: Physics Department, University of Connecticut, Storrs, CT 06269-3046, USA.
§Also: Instituto de Física Corpuscular, CSIC-Universidad de Valencia, P.O. Box 22085, 46071 Valencia, Spain.
‖Deceased.

$$\xi \equiv \frac{f_{B_s}\sqrt{B_{B_s}}}{f_{B_d}\sqrt{B_{B_d}}}. \tag{4}$$

Given improved lattice calculations of the nonperturbative factor ξ, recent experimental measurements of the oscillation frequencies Δm_d and Δm_s to about 1% accuracy [6–9] now allow the possibility of precisely determining the ratio of the CKM matrix elements $|V_{td}|/|V_{ts}|$ (see, for example, Ref. [10]).

The ratio $|V_{td}|/|V_{ts}|$ constrains the apex of the CKM unitarity triangle [11,12]. It is likely that new physics would give rise to new quark-flavor-changing interactions and additional *CP*-violating phases; these would manifest themselves as apparent inconsistencies among different measurements of quantities which should be identical within the standard CKM picture. Thus a precise determination of the ratio ξ will help to constrain physics beyond the standard model. Furthermore, possible indications of new physics in B_d^0-mixing at the ∼2.7-σ level [13] make the lattice calculation of *B*-meson mixing parameters timely.

Recently, the HPQCD Collaboration published the first unquenched determination of ξ with an accuracy of 2.6% [14], and the Fermilab Lattice and MILC Collaborations expect to have a result with similar errors soon [15]. The HPQCD calculation employs a nonrelativistic QCD (NRQCD) action for the heavy *b*-quark [16], while the Fermilab/MILC calculation uses the relativistic "Fermilab" action for the *b*-quark [17]. Both of these computations, however, rely on the same "2 + 1" flavor asqtad-improved staggered ensembles generated by the MILC Collaboration [18], which include the effects of two degenerate light quarks and one heavier close-to-strange quark in the sea sector.

For such a phenomenologically important quantity as ξ, it is valuable to have an independent cross check using different formulations of the lattice action for both the light and heavy quarks. Our calculation employs the 2 + 1 flavor dynamical domain-wall ensembles generated by the RBC and UKQCD Collaborations with a lattice spacing of $a \approx 0.11$ fm $(a^{-1} = 1.729$ GeV) [19]. The use of domain-wall fermions [20–22] has the advantage over other light-quark formulations that the chiral perturbation theory expressions needed to extrapolate domain-wall lattice results to the physical *u*- and *d*-quark masses are closer to the continuum forms and have fewer parameters than in the Wilson or staggered cases [23,24]. We compute the *b*-quarks in the static limit $(m_b \to \infty)$, which leads to correlation functions that are noisier than those with propagating *b*-quarks such as in the Fermilab [17] or NRQCD actions [16]. We therefore use the static-quark formulation of Refs. [25,26] with either APE [27,28] or HYP [29] smearing of the static-quark gauge links to increase the signal-to-noise ratio and reduce scaling violations (for some quantities) as compared to the Eichten-Hill action

[30]. Furthermore, the approximate chiral symmetry of the domain-wall action combined with the spin symmetry of the static action simplifies the lattice-to-continuum operator matching as compared to the Wilson case by reducing the number of additional lattice operators which appear [31,32]. The results of this work extend an earlier study with two flavors of dynamical quarks and heavier light-quark masses in Ref. [33].

The primary purpose of this paper is to demonstrate the viability of our method for computing the *B*-meson decay constants and $\Delta B = 2$ mixing matrix elements. We therefore use the small-volume (16^3) ensembles with only one lattice spacing and have relatively heavy light-quark masses and limited statistics. A novel feature of this work is the use of SU(2) heavy-light meson chiral perturbation theory (HMχPT) to extrapolate $N_f = 2 + 1$ lattice QCD results for *B*-meson quantities to the physical quark masses. This follows the approach taken by the RBC and UKQCD Collaborations in the light pseudoscalar meson sector in Ref. [34], and differs from the calculations of HPQCD and Fermilab/MILC, both of whom use SU(3) HMχPT for their chiral and continuum extrapolations [14,15]. The use of SU(2) χPT is based on on the fact that the strange quark is much heavier than the up and down quarks, and can therefore be integrated out of the chiral effective theory. Because lattice QCD simulations at the physical strange-quark mass are possible via tuning, interpolation, or reweighting, SU(3) χPT is generally not needed to extrapolate the strange quark to its physical value. When the masses of the light valence and sea quarks are sufficiently small such that SU(2) chiral perturbation theory is applicable, SU(2) χPT for light pseudoscalar meson masses and decay constants converges more rapidly than SU(3) χPT [34–37]. Although we do not have enough data or sufficiently light quark masses to perform a thorough comparison of SU(2) and SU(3) HMχPT in this work, we believe that the use of SU(2) HMχPT provides a promising alternative to SU(3) and warrants further study when better data is available.

In this work we compute both the ratio of decay constants, f_{B_s}/f_{B_d}, and the ratio of $\Delta B = 2$ matrix elements, ξ. We focus on the SU(3)-breaking ratios because both the statistical and systematic errors are smaller and under better control than for the individual decay constants and mixing matrix elements. Our results have large total uncertainties compared to those of HPQCD and Fermilab/MILC. Within errors, however, our results for the SU(3)-breaking ratios are consistent with the values presented in the literature and we expect to improve upon them and present values for the individual decay constants and matrix elements in a future work.

This paper is organized as follows. First, in Sec. II, we present the actions and parameters used in our lattice simulations. Next, in Sec. III, we briefly discuss the perturbative matching of the heavy-light current and the four-

fermion operators; the details of the lattice perturbation theory calculation will be presented in another publication [38]. We compute 2-point and 3-point lattice correlation functions and extract the decay constants and mixing matrix elements in Sec. IV, and extrapolate these results to the physical light-quark masses using a phenomenologically-motivated function based on next-to-leading order (NLO) SU(2) heavy-meson chiral perturbation theory in Sec. V. In Sec. VI we estimate the contributions of the various systematic uncertainties to f_{B_s}/f_{B_d} and ξ, discussing each item in the error budget separately. We present our final results and conclude in Sec. VII.

This paper also contains four appendices. Appendix A specifies the SU(3) projection methods that are used in our APE and HYP-smeared gauge links. In Appendix B some details of the perturbative formulas used to match from continuum QCD to HQET as well as for the HQET running are presented. Appendix C discusses the large ground state degeneracy present in HQET and how it can be exploited to compute B-meson mixing matrix elements using localized sources and sinks. The SU(3) and SU(2) NLO HMχPT expressions for the B-meson decay constants and mixing matrix elements relevant for $N_f = 2 + 1$ domain-wall lattice simulations are provided in Appendix D; some of these results have not been presented previously in the literature.

II. LATTICE ACTIONS AND PARAMETERS

In this section we briefly describe our numerical lattice simulations. We use the unquenched lattices generated by the RBC and UKQCD Collaborations which include the effects of $2 + 1$ dynamical flavors of domain-wall quarks [19]. We calculate the decay constants and matrix elements on configurations with a lattice spacing of $a^{-1} = 1.729(28)$ GeV [34] and an approximate spatial volume of $L^3 \approx (1.8 \text{ fm})^3$. For each ensemble, the masses of the up and down sea quarks are degenerate and the mass of the strange sea quark is slightly larger than its physical value. In order to distinguish the dynamical quark masses used in our simulations from the physical u, d, and s-quark masses, we denote the lighter sea quark mass by m_l and the heavier sea quark mass by m_h. Our lightest pion mass is approxi-

TABLE I.   Available $2 + 1$ flavor domain-wall ensembles [19]. The columns from left to right are the approximate lattice spacing in fm, the bare light and strange quark masses in the sea sector, the dimensions of the lattice in lattice units, the pion mass in the sea sector, the dimensionless factor $m_\pi L$, and the residual quark mass in the chiral limit.

a (fm)	am_l/am_h	Volume	m_π (MeV)	$m_\pi L$	am_{res}
≈ 0.11	$0.01/0.04$	$16^3 \times 32$	430	3.9	0.003 15
≈ 0.11	$0.02/0.04$	$16^3 \times 32$	560	5.2	0.003 15
≈ 0.11	$0.03/0.04$	$16^3 \times 32$	670	6.3	0.003 15

mately 430 MeV. Table I summarizes the parameters of the dynamical domain-wall ensembles used in our analyses.

In Sec. II A we present the domain-wall fermion action used for both the valence and sea light u, d, and s quarks. Next, in Sec. II B, we show the Iwasaki gauge action used for the gluon fields. Finally, we discuss the static action used for the heavy b quarks in Sec. II C.

A. Light-quark action

We use the five-dimensional domain-wall fermion action [21,22] for the light u, d, and s quarks in both the valence and sea sectors:

$$S_{\text{DW}} = a^4 \left(\sum_{s,s'=0}^{L_s-1} \sum_{x,y} \bar{\psi}_s(x) D_{ss'}^{\text{DW}}(x, y) \psi_{s'}(y) - \sum_x m_f \bar{q}(x) q(x) \right), \tag{5}$$

$$D_{ss'}^{\text{DW}}(x, y) = D^4(x, y) \delta_{s,s'} + D^5(s, s') \delta_{x,y} + a^{-1}(M_5 - 5) \delta_{s,s'} \delta_{x,y}, \tag{6}$$

$$D^4(x, y) = \sum_\mu \frac{1}{2a} [(1 - \gamma_\mu) U_\mu(x) \delta_{x+\hat{\mu},y} + (1 + \gamma_\mu) U_\mu^\dagger(y) \delta_{x-\hat{\mu},y}], \tag{7}$$

$$D^5(s, s') = \begin{cases} a^{-1} P_L \delta_{1,s'} & (s = 0) \\ a^{-1}(P_L \delta_{s+1,s'} + P_R \delta_{s-1,s'}) & (0 < s < L_s - 1) \\ a^{-1} P_R \delta_{L_s-2,s'} & (s = L_s - 1) \end{cases} \tag{8}$$

where $\psi_s(x)$ is a 5-d Wilson-type fermion field. The fifth dimension extends from 0 to $L_s - 1$ and is labeled by s. The domain-wall height is set to $M_5 = 1.8$ in our simulations. The projectors $P_L = (1 - \gamma_5)/2$ and $P_R = (1 + \gamma_5)/2$ select left- and right-handed spinor components, respectively. The physical four-dimensional quark field $q(x)$ is constructed from the five-dimensional field

$\psi_s(x)$ at $s = 0$ and $L_s - 1$:

$$q(x) = P_L \psi_0(x) + P_R \psi_{L_s-1}(x), \tag{9}$$

$$\bar{q}(x) = \bar{\psi}_0(x) P_R + \bar{\psi}_{L_s-1}(x) P_L. \tag{10}$$

In the limit $L_s \to \infty$, the left-handed and right-handed modes decouple and exact chiral symmetry is recovered. In

practice, however, L_s is large but finite in numerical lattice simulations. This leads to a small amount of chiral symmetry breaking which can be parameterized in terms of an additive shift to the bare domain-wall quark mass. At the value $L_s = 16$ used in our simulations we obtain a residual quark mass of $am_{res} = 0.003\,15(2)$ [34]. Because mixing between heavy-light four-fermion operators of different chiralities is proportional to the value of am_{res}, this indicates that the size of errors from mixing with wrong-chirality operators is negligible.

B. Gluon action

We use the Iwasaki gauge action for the gluons [39]:

$$S_{gauge} = -\frac{\beta}{3}\left((1 - 8c_1)\sum_P \mathrm{Re\,Tr}[U_P] + c_1 \sum_R \mathrm{Re\,Tr}[U_R]\right),$$

(11)

where $\beta \equiv 6/g_0^2$ and g_0 is the bare lattice coupling. U_P is the path-ordered product of gauge links around the 1×1 plaquette P and U_R is the path-ordered product of gauge links around the 1×2 rectangle R. The constant c_1 is set to -0.331 in the Iwasaki action and we use $\beta = 2.13$ in our simulations. As was shown in Refs. [40,41] for the quenched approximation, the use of the Iwasaki action in combination with domain-wall valence quarks leads to improved chiral symmetry and a smaller residual quark mass than for the Wilson gauge action [42]. In the case of $N_f = 2 + 1$ dynamical domain-wall simulations, the use of the Iwasaki action also allows frequent tunneling between topological sectors [43].

C. Heavy-quark action

We use an improved static action for the b-quarks in the 2-point and 3-point correlation functions needed to compute the decay constants and matrix elements. We build upon the original lattice formulation of the static effective action that was constructed by Eichten and Hill [44]:

$$S_{static} = a^3 \sum_{x,y} (\bar{h}(x)[\delta_{x,y} - U_0^\dagger(y)\delta_{x-\hat{0},y}]P_+ h(y)$$
$$- \bar{h}(x)[\delta_{x,y} - U_0(x)\delta_{x+\hat{0},y}]P_- h(y)),$$

(12)

where $h(x)$ is the static quark field at site x, $U_0(x)$ is the gauge link in the temporal direction and $\hat{0}$ denotes the unit vector along the temporal direction. The projectors $P_\pm = \frac{1}{2}(1 \pm \gamma_0)$ select the parity even and odd components of $h(x)$, which we denote by $h^{(+)}(x)$ and $h^{(-)}(x)$. respectively. The components of the static-quark field $h^{(\pm)}$ in the Eichten-Hill action satisfy the relation $\gamma_0 h^{(\pm)} = \pm h^{(\pm)}$. Furthermore, the static quark propagator $H(x, y) = \langle h(x)\bar{h}(y)\rangle$ can be expressed as the product of gauge links:

$$H(x, y) = H^+(x, y) + H^-(x, y),$$

(13)

$$H^{(+)}(x, y) = \frac{1}{a^3}\theta(t_x - t_y)$$
$$\times \delta_{\vec{x},\vec{y}}[U_0^\dagger(x - \hat{0})\dots U_0^\dagger(y + \hat{0})U_0^\dagger(y)]P_+,$$

(14)

$$H^{(-)}(x, y) = -\frac{1}{a^3}\theta(t_y - t_x)$$
$$\times \delta_{\vec{x},\vec{y}}[U_0(x)U_0(x + \hat{0})\dots U_0(y - \hat{0})]P_-.$$

(15)

These properties make the Eichten-Hill formulation computationally simple. In practice, however, numerical simulations with this action are quite noisy. Therefore we use instead smeared (or "fat") link actions:

$$S_{fat} = a^3 \sum_{x,y} (\bar{h}(x)[\delta_{x,y} - \bar{V}_0^\dagger(y)\delta_{x-\hat{0},y}]P_+ h(y)$$
$$- \bar{h}(x)[\delta_{x,y} - \bar{V}_0(x)\delta_{x+\hat{0},y}]P_- h(y)),$$

(16)

where the new gauge link $\bar{V}$ is obtained from the thin link U by either APE blocking [27,28] or hypercubic (HYP) blocking [29]. The heavy quark propagator for the improved action is given by

$$H_{fat}^{(+)}(x, y) = \frac{1}{a^3}\theta(t_x - t_y)$$
$$\times \delta_{\vec{x},\vec{y}}[\bar{V}_0^\dagger(x - \hat{0})\dots \bar{V}_0^\dagger(y + \hat{0})\bar{V}_0^\dagger(y)]P_+,$$

(17)

$$H_{fat}^{(-)}(x, y) = -\frac{1}{a^3}\theta(t_y - t_x)$$
$$\times \delta_{\vec{x},\vec{y}}[\bar{V}_0(x)\bar{V}_0(x + \hat{0})\dots \bar{V}_0(y - \hat{0})]P_-.$$

(18)

The replacement of the simple gauge link U_0 by a smeared link significantly improves the signal-to-noise ratio [26].

We construct the fattened APE link by adding a weighted sum of the staples to the original thin link, and restrict the smearing to links in the temporal direction along which the heavy quark propagates. We use the APE parameter $\alpha = 1$, for which the smeared link is given by [28]

$$\bar{V}_0(x) = \mathbf{Proj}_{SU(3)}[V_0(x)],$$

(19)

$$V_0(x) = \frac{1}{6}\sum_{\nu=1}^{3}(U_\nu(x)U_0(x + \hat{\nu})U_\nu^\dagger(x + \hat{0})$$
$$+ U_\nu^\dagger(x - \hat{\nu})U_0(x - \hat{\nu})U_\nu(x + \hat{0} - \hat{\nu})).$$

(20)

We build the HYP link from three iterative steps of APE smearing which are restricted to the hypercube around the original link. For links in the temporal direction the construction is as follows:

$$\bar{V}_0(x) = \mathbf{Proj}_{\mathrm{SU(3)}}\Bigg[(1 - \alpha_1)U_0(x) + \frac{\alpha_1}{6}$$
$$\times \sum_{\nu=\pm 1}^{\pm 3} \tilde{V}_{\nu;0}(x)\tilde{V}_{0;\nu}(x + \hat{\nu})\tilde{V}_{\nu;0}^\dagger(x + \hat{0})\Bigg], \quad (21)$$

$$\tilde{V}_{\mu;\nu}(x) = \mathbf{Proj}_{\mathrm{SU(3)}}\Bigg[(1 - \alpha_2)U_\mu(x) + \frac{\alpha_2}{4}$$
$$\times \sum_{\substack{\rho=\pm 0 \\ \rho \neq \mu,\nu}}^{\pm 3} V_{\rho;\nu\mu}(x)V_{\mu;\rho\nu}(x + \hat{\rho})V_{\rho;\nu\mu}^\dagger(x + \hat{\mu})\Bigg], \tag{22}$$

$$V_{\mu;\nu\rho}(x) = \mathbf{Proj}_{\mathrm{SU(3)}}\Bigg[(1 - \alpha_3)U_\mu(x) + \frac{\alpha_3}{2}$$
$$\times \sum_{\substack{\eta=\pm 0 \\ \eta \neq \mu,\nu,\rho}}^{\pm 3} U_\eta(x)U_\mu(x + \hat{\eta})U_\eta^\dagger(x + \hat{\mu})\Bigg]. \tag{23}$$

We use the HYP smearing parameters $(\alpha_1, \alpha_2, \alpha_3) = (1.0, 1.0, 0.5)$, sometimes referred to as HYP2. These were shown to approximately minimize the noise-to-signal ratio in Ref. [25].

In Eqs. (19)–(23) $\mathbf{Proj}_{\mathrm{SU(3)}}(V)$ indicates the projection of the link V onto an SU(3) matrix. This projection reduces the statistical noise and thus enhances the smearing effect without increasing the level of smearing. In some cases the SU(3) projection also suppresses quantum corrections to lattice operators in perturbation theory [45]. The projection of the smeared link onto SU(3) is not unique, and we use two different schemes: for the case of APE smearing, Eq. (19), we project by the unit circle method based on polar decomposition [46], while for the case of HYP smearing, Eqs. (21)–(23), we obtain the projected matrix by an iterative procedure seeking the SU(3) matrix $U_{\max}$ that maximizes $\mathrm{Re}\,\mathrm{Tr}(U_{\max}V^\dagger)$, where V is the HYP smeared link matrix [47]. We describe the details of the two schemes and show their equivalence in the weak coupling limit in Appendix A.

III. PERTURBATIVE MATCHING OF HEAVY-LIGHT CURRENT AND FOUR-FERMION OPERATORS

In order to renormalize the heavy-light axial current and $\Delta B = 2$ four-fermion operator, we adopt a two-step matching procedure. In the first step, we match the QCD operators renormalized in the $\overline{\mathrm{MS}}$ scheme using naive dimensional regularization (NDR) at a scale μ_b to continuum static effective theory operators renormalized at a scale μ. This step is described in Sec. III A. In this paper, we choose μ_b to be the b-quark mass m_b and μ to be the inverse lattice spacing a^{-1}. In the second step, we match the continuum static effective theory operators to the lattice ones. This step is described in Sec. III B. We combine the

results of the two steps and present the results for the complete matching coefficients in Table III.

A. Continuum matching

The QCD operators considered in this paper are the axial vector current

$$A_0^{\mathrm{QCD}} = \bar{b}\gamma_0\gamma_5 q, \tag{24}$$

and the $\Delta B = 2$ four-quark operator

$$O_L^{\mathrm{QCD}}(\mu_b) = [\bar{b}\gamma_\mu(1 - \gamma_5)q][\bar{b}\gamma_\mu(1 - \gamma_5)q]. \tag{25}$$

These are related to the continuum HQET operators by

$$A_0^{\mathrm{QCD}} = C_A(\mu)A_0^{\mathrm{HQET}}(\mu) + O(\Lambda_{\mathrm{QCD}}/m_b), \tag{26}$$

$$O_L^{\mathrm{QCD}}(\mu_b) = Z_1(\mu_b, \mu)O_L^{\mathrm{HQET}}(\mu) + Z_2(\mu_b, \mu)O_S^{\mathrm{HQET}}(\mu) + O(\Lambda_{\mathrm{QCD}}/m_b), \tag{27}$$

where

$$A_0^{\mathrm{HQET}} = \bar{h}\gamma_0\gamma_5 q, \tag{28}$$

$$O_L^{\mathrm{HQET}} = [\bar{h}\gamma_\mu(1 - \gamma_5)q][\bar{h}\gamma_\mu(1 - \gamma_5)q], \tag{29}$$

$$O_S^{\mathrm{HQET}} = [\bar{h}(1 - \gamma_5)q][\bar{h}(1 - \gamma_5)q]. \tag{30}$$

Note that, because A_0^{QCD} is a conserved current, it does not depend upon the renormalization scale μ_b. The coefficients C_A and $\vec{Z} = (Z_1, Z_2)$ in Eqs. (26) and (27) are products of three factors:

$$C_A(\mu) = \tilde{C}_A(m_b) \cdot U_A^{(4)}(m_b, m_c) \cdot U_A^{(3)}(m_c, \mu), \tag{31}$$

$$\vec{Z}(\mu_b, \mu) = \vec{\tilde{Z}}(\mu_b, m_b) \cdot U_L^{(4)}(m_b, m_c) \cdot U_L^{(3)}(m_c, \mu), \tag{32}$$

where $\tilde{C}_A$ and $\vec{\tilde{Z}} \equiv (\tilde{Z}_1, \tilde{Z}_2)$ are the matching coefficients from HQET to QCD. The factors $U_A^{(N_f)}(\mu', \mu)$ and the 2×2 matrix $U_L^{(N_f)}(\mu', \mu)$ account for the renormalization group running between scales: We first match the continuum QCD operators onto continuum HQET operators at one-loop; this occurs at a scale $\mu_b = m_b$ in the $\overline{\mathrm{MS}}$(NDR) scheme. We then run the matching coefficients in four-flavor continuum HQET from m_b to m_c at two-loops. Finally, we run the coefficients at two-loops in three-flavor continuum HQET from m_c to the scale $\mu = 1/a$, where the matching to three-flavor lattice HQET is done.

The matching factors and anomalous dimensions needed to compute these coefficients are given in Refs. [30,48,49] for the heavy-light current and in Refs. [50–53] for the four-quark operator. For completeness, we present them in Appendix B. Here we simply quote the results for the matching coefficients, which already contain some terms of $O(\alpha_s^2)$:

$$C_A(\mu) = \left[\frac{\alpha_s(m_b)}{\alpha_s(m_c)}\right]^{-(6/25)} \cdot \left[\frac{\alpha_s(m_c)}{\alpha_s^{(3)}(\mu)}\right]^{-(2/9)} \cdot \left(1 - \frac{8}{3}\frac{\alpha_s(m_b)}{4\pi}\right) \cdot \left(1 + J_A^{(4)}\frac{\alpha_s(m_b) - \alpha_s(m_c)}{4\pi}\right)$$
$$\cdot \left(1 + J_A^{(3)}\frac{\alpha_s(m_c) - \alpha_s^{(3)}(\mu)}{4\pi}\right) + \mathcal{O}(\alpha_s^2), \tag{33}$$

$$Z_1(m_b, \mu) = \left[\frac{\alpha_s(m_b)}{\alpha_s(m_c)}\right]^{-(12/25)} \cdot \left[\frac{\alpha_s(m_c)}{\alpha_s^{(3)}(\mu)}\right]^{-(4/9)} \cdot \left\{\left(1 - 14\frac{\alpha_s(m_b)}{4\pi}\right) \cdot \left(1 + J_{11}^{(4)}\frac{\alpha_s(m_b) - \alpha_s(m_c)}{4\pi}\right)\right.$$
$$\cdot \left(1 + J_{11}^{(3)}\frac{\alpha_s(m_c) - \alpha_s^{(3)}(\mu)}{4\pi}\right) + 2\frac{\alpha_s(m_b)}{4\pi}\left\{\left(1 - \left[\frac{\alpha_s(m_b)}{\alpha_s(m_c)}\right]^{8/25}\right)\left(1 + J_{11}^{(3)}\frac{\alpha_s(m_c) - \alpha_s^{(3)}(\mu)}{4\pi}\right)\right.$$
$$\left.\left. + \left[\frac{\alpha_s(m_b)}{\alpha_s(m_c)}\right]^{8/25} \cdot \left(1 - \left[\frac{\alpha_s(m_c)}{\alpha_s^{(3)}(\mu)}\right]^{8/27}\right)\right\}\right\} + \mathcal{O}(\alpha_s^2), \tag{34}$$

$$Z_2(m_b, \mu) = -8\frac{\alpha_s(m_b)}{4\pi}\left[\frac{\alpha_s(m_b)}{\alpha_s(m_c)}\right]^{-(4/25)}\left[\frac{\alpha_s(m_c)}{\alpha_s^{(3)}(\mu)}\right]^{-(4/27)} + \mathcal{O}(\alpha_s^2), \tag{35}$$

with the parameters J_A and J_{11} given by

$$J_A^{(3)} = -0.7545, \qquad J_A^{(4)} = -0.9098, \tag{36}$$

$$J_{11}^{(3)} = -1.6980, \qquad J_{11}^{(4)} = -1.8637. \tag{37}$$

Note that the leading-order mixing between O_L^{QCD} and O_S^{HQET} is of $\mathcal{O}(\alpha_s)$. To determine the coupling constant α_s at different scales, which is required to obtain these results, we fix the value of α_s at the Z-boson mass to the PDG value $\alpha_s(m_Z = 91.1876 \text{ GeV}) = 0.1176$ [6]. Using four-loop running [54,55], we obtain $\alpha_s(m_b = 4.20 \text{ GeV}[6]) = 0.2228$, $\alpha_s(m_c = 1.27 \text{ GeV}[6]) = 0.3819$, and $\alpha_s^{(3)}(a^{-1} = 1.729 \text{ GeV}[34]) = 0.3141$. Hence we find

$$C_A(a^{-1}) = 1.0459, \qquad Z_1(m_b, a^{-1}) = 0.9100,$$
$$Z_2(m_b, a^{-1}) = -0.1502 \tag{38}$$

for the matching coefficients in Eqs. (26) and (27) that relate the operators in continuum QCD to those in the continuum static effective theory.

B. Static effective theory matching

We next discuss the lattice-to-continuum operator matching in the static effective theory. Although both the domain-wall and static quark actions are on-shell $\mathcal{O}(a)$ improved, the domain-wall-static vertices still receive $\mathcal{O}(a)$ corrections. This was shown in Ref. [56] for the case of clover light quarks and static heavy quarks even when the parameter in the clover action $r \to 0$ and chiral symmetry is restored in the light-quark sector. In this work, we remove $\mathcal{O}(a)$ lattice discretization errors from the axial vector current in the light-quark chiral limit at one-loop in lattice perturbation theory by adding dimension-four operators containing derivatives; we refer to these errors as $\mathcal{O}(pa)$ to distinguish them from $\mathcal{O}(m_q a)$ errors that vanish

in the light-quark chiral limit. The improved operators are determined by requiring that the on-shell quark scattering amplitudes in the B-meson rest frame agree in the lattice and continuum theories through $\mathcal{O}(\alpha_s pa)$, where p is the momenta of the light quarks in the B-meson and is typically of $\mathcal{O}(\Lambda_{\text{QCD}})$. The details of this calculation are presented in Ref. [38]. We neglect $\mathcal{O}(m_q a)$ errors because these are estimated to be small [38], but account for them when estimating the systematic errors in Sec. VI. In this work we also neglect $\mathcal{O}(\alpha_s pa)$ corrections to the four-quark operator since we estimate the size of the resulting contribution to the SU(3) breaking ratio ξ would be much smaller than our current statistical precision, but we again account for them in the systematic error budget. The one-loop $\mathcal{O}(\alpha_s pa)$ corrections for the four-quark operator are available in Ref. [38], however, for use in future simulations.

For domain-wall light quarks, the one-loop lattice perturbation theory calculations are presented in Refs. [32,38,57]. The lattice-to-continuum matching has the form:

$$A_0^{\text{HQET}}(\mu) = \frac{\sqrt{u_0}}{\sqrt{(1 - (w_0^{\text{MF}})^2)Z_w^{\text{MF}}}}Z_A^{\text{MF}}(\mu, a^{-1})$$
$$\times [A_0^{\text{lat}}(a^{-1}) + c_A^{\text{MF}}(\mu, a^{-1})aA_{\partial,0}^{\text{lat}}(a^{-1})]$$
$$\equiv Z_A^{\text{MF}}(\mu, a^{-1})$$
$$\times [A_0^{\text{lat}}(a^{-1}) + c_A^{\text{MF}}(\mu, a^{-1})aA_{\partial,0}^{\text{lat}}(a^{-1})]. \tag{39}$$

$$O_L^{\text{HQET}}(\mu) = \frac{u_0}{(1 - (w_0^{\text{MF}})^2)Z_w^{\text{MF}}}Z_L^{\text{MF}}(\mu, a^{-1})O_L^{\text{lat}}(a^{-1})$$
$$\equiv Z_L^{\text{MF}}(\mu, a^{-1})O_L^{\text{lat}}(a^{-1}), \tag{40}$$

$$O_S^{\text{HQET}}(\mu) = \frac{u_0}{(1 - (w_0^{\text{MF}})^2)}O_S^{\text{lat}}(a^{-1})$$
$$\equiv Z_S^{\text{MF}}(\mu, a^{-1})O_S^{\text{lat}}(a^{-1}), \tag{41}$$

with the constant

$$w_0^{\mathrm{MF}} = 1 - M_5 + 4(1 - u_0), \qquad (42)$$

where the mean-field link $u_0 = P^{1/4}$ is obtained from the expectation value of the plaquette P. In Eqs. (39)–(41) we match A^{HQET} and O_L^{HQET} at one-loop, but match O_S^{HQET} at tree level. This is sufficient because the leading-order mixing between the continuum QCD operator O_L^{QCD} and the continuum HQET operator O_S^{HQET} is already of $\mathcal{O}(\alpha_s)$, and has no tree-level component. The lattice operators have the same form as in the continuum static effective theory

$$A_0^{\mathrm{lat}} = \bar{h}\gamma_0\gamma_5 q, \qquad (43)$$

$$O_L^{\mathrm{lat}} = [\bar{h}\gamma_\mu(1 - \gamma_5)q][\bar{h}\gamma_\mu(1 - \gamma_5)q], \qquad (44)$$

$$O_S^{\mathrm{lat}} = [\bar{h}(1 - \gamma_5)q][\bar{h}(1 - \gamma_5)q]. \qquad (45)$$

The $O(pa)$ derivative operator in the equation for the axial current is given by

$$A_{\partial,0}^{\mathrm{lat}} = \partial_0(\bar{h}\gamma_5 q), \qquad (46)$$

where we have simplified the expression using the equations-of-motion. The domain-wall specific renormalization factor Z_w^{MF} that enters the above equations was calculated perturbatively in Ref. [58].

The superscript "MF" denotes mean-field improvement [59], in which we modify the bare lattice coupling using the value of the mean-field link. Use of this "boosted" coupling as the new expansion parameter improves the convergence of lattice perturbation theory. The mean-field improved coupling α^{MF} has several definitions which differ only at higher-order in perturbation theory than we consider. These differences enter our estimate of the systematic error in Sec. VI. Our choice for obtaining the mean-field improved coupling from the bare lattice coupling g_0^2 is

$$\frac{1}{(g^{\mathrm{MF}})^2} = \frac{P}{g_0^2} + d_g + c_p + N_f d_f, \qquad (47)$$

where $N_f = 3$ is the number of dynamical flavors. We use the plaquette value averaged over different light sea quark mass, $P = 0.5881$, because the difference in the value of P for different light sea quark masses is less than 0.05% for the ensembles used in this work. The constants $d_g = 0.1053$ and $c_p = 0.1401$ were calculated for the Iwasaki gauge action in Ref. [58] and $d_f = -0.001465$ was obtained for $M_5^{\mathrm{MF}} = 1.303$ from a linear interpolation of the results in Table II of Ref. [60]. On our ensembles, the mean-field improved coupling is $\alpha^{\mathrm{MF}} = 0.1769$.

Given the value of the plaquette in our simulations, $u_0 = 0.8757$ and $w_0^{\mathrm{MF}} = -0.3029$. After setting $\mu = a^{-1}$, the coefficients appearing in Eqs. (39)–(41) are

$$Z_w^{\mathrm{MF}} = 1 + \frac{\alpha^{\mathrm{MF}}}{4\pi}\frac{4}{3} \times 5.250, \qquad (48)$$

TABLE II. Lattice-to-continuum operator matching factors in the static effective theory for the choice of coupling α_s^{MF}.

Smearing	$\mathcal{Z}_A^{\mathrm{MF}}$	c_A^{MF}	$\mathcal{Z}_L^{\mathrm{MF}}$	$\mathcal{Z}_S^{\mathrm{MF}}$
APE	0.9090	0.0653	0.8225	0.9642
HYP	0.9382	0.1204	0.8909	0.9642

$$Z_A^{\mathrm{MF}} = 1 + \frac{\alpha^{\mathrm{MF}}}{4\pi}\frac{4}{3} \times \begin{cases} -1.584 & \mathrm{APE} \\ 0.077 & \mathrm{HYP} \end{cases} \qquad (49)$$

$$c_A^{\mathrm{MF}} = \frac{\alpha^{\mathrm{MF}}}{4\pi}\frac{4}{3} \times \begin{cases} 3.480 & \mathrm{APE} \\ 6.412 & \mathrm{HYP} \end{cases} \qquad (50)$$

$$Z_L^{\mathrm{MF}} = 1 + \frac{\alpha^{\mathrm{MF}}}{4\pi} \times \begin{cases} -4.462 & \mathrm{APE} \\ 1.076 & \mathrm{HYP} \end{cases} \qquad (51)$$

where the values are given for both the APE and HYP link-smearings used in this work. These results can be combined to determine the overall multiplicative renormalization factors denoted by $\mathcal{Z}$ in Eqs. (39)–(41) which we present for completeness in Table II.

C. Complete matching coefficients

In order to match the lattice HQET operators at scale $\mu = a^{-1}$ directly onto the desired continuum QCD operators at $\mu_b = m_b$, we must combine the coefficients obtained in the two steps. We define the complete lattice HQET-to-continuum QCD matching coefficients as

$$Z_\Phi(a^{-1}) = C_A(a^{-1}) \cdot \mathcal{Z}_A^{\mathrm{MF}}(a^{-1}, a^{-1}), \qquad (52)$$

$$Z_{\mathrm{VA}}(\mu_b, a^{-1}) = Z_1(\mu_b, a^{-1}) \cdot \mathcal{Z}_L^{\mathrm{MF}}(a^{-1}, a^{-1}), \qquad (53)$$

$$Z_{\mathrm{SP}}(\mu_b, a^{-1}) = Z_2(\mu_b, a^{-1}) \cdot \mathcal{Z}_S^{\mathrm{MF}}(a^{-1}, a^{-1}), \qquad (54)$$

and present their values for our choice of simulation parameters in Table III. These will be used in the following section to extract the physical decay constants and $\Delta B = 2$ four-fermion matrix elements via the relations

$$A_0^{\mathrm{QCD}} = Z_\Phi(a^{-1})(A_0^{\mathrm{lat}}(a^{-1}) + c_A^{\mathrm{MF}}aA_{\partial,0}^{\mathrm{lat}}(a^{-1})), \qquad (55)$$

$$\begin{aligned} O_L^{\mathrm{QCD}}(\mu_b) &= Z_{\mathrm{VA}}(\mu_b, a^{-1})O_L^{\mathrm{lat}}(a^{-1}) \\ &\quad + Z_{\mathrm{SP}}(\mu_b, a^{-1})O_S^{\mathrm{lat}}(a^{-1}). \end{aligned} \qquad (56)$$

TABLE III. Perturbative matching factors for the decay constants and mixing matrix elements evaluated for APE smeared and HYP smeared static-quark gauge links for the choices of the strong coupling constant α_s^{MF}.

Smearing	Z_Φ	Z_{VA}	Z_{SP}
APE	0.9507	0.7485	-0.1448
HYP	0.9813	0.8108	-0.1448

In practice, the renormalization factor Z_Φ cancels in the ratio f_{B_s}/f_{B_d}, and only the quantity Z_{SP}/Z_{VA} enters the ratio ξ. Therefore, we do not need Z_Φ (or Z_{VA} and Z_{SP} by themselves) for our current analysis of the SU(3)-breaking ratios. We present all three matching coefficients for completeness, however, because they will be necessary for calculating the individual decay constants and four-fermion operator-mixing matrix elements in future work.

IV. LATTICE CALCULATION OF SU(3) BREAKING RATIOS

In this section we calculate the ratios of the B-meson decay constants and mixing matrix elements at unphysical values of the light and strange quark masses. On each sea-quark ensemble, we compute the necessary 2-point and 3-point correlation functions at two values of the valence quark mass: the unitary point $m_x = m_l$ and a point tuned to the physical strange quark mass $am_s = 0.0359$ [19]. We also use two different link smearings (APE and HYP) to improve the static heavy quark action in order to help estimate discretization effects. Table IV presents the parameters chosen for our matrix element computations. In the first subsection we calculate the ratio of B-meson decay constants and in the second we calculate the ratio of $\Delta B = 2$ mixing matrix elements.

A. Calculation of the ratio of B-meson decay constants

In QCD the decay constant f_{B_q} for the B_q-meson is defined by the vacuum-to-meson matrix element

$$\langle 0|\bar{b}\gamma_\mu\gamma_5 q|B_q(p)\rangle = if_{B_q}p_\mu. \tag{57}$$

Because the decay constant f_{B_q} behaves as $1/\sqrt{m_{B_q}}$ in the limit of large B_q-meson mass, we calculate the combined decay amplitude

$$\Phi_{B_q} = f_{B_q}\sqrt{m_{B_q}}, \tag{58}$$

where m_{B_q} is the physical mass of the B_q-meson. We determine the quantity Φ_{B_q} by computing two-point correlation functions of the static-light axial current $A_\mu^{(\pm)\mathrm{stat}} = \bar{h}^{(\pm)}\gamma_\mu\gamma_5 q$.[1]

In practice, we use Coulomb gauge-fixed wall sources for the b-quark to calculate the local-wall (LW) and wall-wall (WW) correlation functions

$$\mathcal{C}^{\mathrm{LW}}(t, t_0) = a^3 \sum_{\vec{x}\in V}\langle 0|A_0^L(\vec{x}, t)A_0^W(t_0)^\dagger|0\rangle, \tag{59}$$

$$\mathcal{C}^{\mathrm{WW}}(t, t_0) = \langle 0|A_0^W(t)A_0^W(t_0)^\dagger|0\rangle, \tag{60}$$

---

[1]For the case of static b-quarks, we can relate the B-meson interpolating operator $\bar{h}^{(-)}\gamma_5 q$ to the axial current operator in the temporal direction using the relation $h^{(\pm)}(x)\gamma_0 = \pm h^{(\pm)}(x)$, and thereby express all correlation functions entirely in terms of the axial current.

TABLE IV. Parameters used in our simulations. The columns from left to right are the light and (approximately) strange sea quark masses, the light and strange valence quark masses, and the number of configurations analyzed for both of our setups using APE or HYP link smearing in the static quark gauge links.

		No. of configs.	
am_l/am_h	am_x	APE	HYP
0.01/0.04	0.01, 0.0359	298	300
0.02/0.04	0.02, 0.0359	298	300
0.03/0.04	0.03, 0.0359	298	300

with the local (L) and wall-source (W) axial currents given by

$$A_0^L(\vec{x}, t) = \bar{h}^{(+)}(\vec{x}, t)\gamma_0\gamma_5 q(\vec{x}, t) + \bar{h}^{(-)}(\vec{x}, t)\gamma_0\gamma_5 q(\vec{x}, t), \tag{61}$$

$$A_0^W(t) = a^6 \sum_{\vec{y}\in V}\sum_{\vec{z}\in V}(\bar{h}^{(+)}(\vec{y}, t)\gamma_0\gamma_5 q(\vec{z}, t) + \bar{h}^{(-)}(\vec{y}, t)\gamma_0\gamma_5 q(\vec{z}, t)). \tag{62}$$

From the ratio of $\mathcal{C}^{\mathrm{LW}}$ to $\mathcal{C}^{\mathrm{WW}}$ we obtain the combined decay amplitude

$$\Phi_{B_q}^{\mathrm{lat}} = \lim_{t\gg t_0}\sqrt{\frac{2}{L^3}}\frac{|\mathcal{C}^{\mathrm{LW}}(t, t_0)|}{\sqrt{\mathcal{C}^{\mathrm{WW}}(t, t_0)e^{-m_{B_q}^*(t-t_0)}}}, \tag{63}$$

where we determine the unphysical B-meson rest mass $m_{B_q}^*$ via

$$am_{B_q}^* = \lim_{t\gg t_0}\log\left(\frac{\mathcal{C}^{\mathrm{LW}}(t, t_0)}{\mathcal{C}^{\mathrm{LW}}(t + a, t_0)}\right). \tag{64}$$

A derivation of Eq. (63) is presented in Appendix C. Finally we compute the renormalized decay amplitude

$$\Phi_{B_q}^{\mathrm{ren}} = Z_\Phi[1 + c_A^{\mathrm{MF}}\sinh(am_{B_q}^*)]\Phi_{B_q}^{\mathrm{lat}}, \tag{65}$$

using the perturbative matching factors given in Tables II and III. The contribution proportional to c_A^{MF} improves the heavy-light axial current operator through $\mathcal{O}(\alpha_s pa)$, where the sinh arises from the symmetric derivative in the $\mathcal{O}(pa)$ operator. The overall multiplicative factor Z_Φ is needed to obtain the combined decay amplitude in the continuum.

The computation of the statistical errors throughout this paper follows the prescription for numerically computing the autocorrelation function as proposed in Ref. [61]. The autocorrelation function quantifies the degree of correlation between two measurements made at different trajectories, and depends upon the observable of interest. By summing the autocorrelation function over the separation between measurements, one obtains the integrated autocorrelation time. We obtain a better estimate of the true statistical error by inflating the variance of the measured Monte Carlo data using the integrated autocorrelation time.

In many instances we must compute the errors in a quantity which itself depends on several lattice correlators; we refer to this as a derived quantity and refer to the lattice correlators as primary observables. When calculating the errors in a derived quantity, we account for the correlations between primary observables by using the functional dependence of the derived quantity on the primary observables. As a cross check of the statistical error estimate, we compared the results obtained with this approach with those obtained using a single-elimination jackknife procedure; we find that both the central values and statistical errors are consistent between the two error estimation methods.

For example, Fig. 1 shows the determinations of $m_{B_q}^*$ and $\Phi_{B_q}^{\mathrm{ren}}$ on the $am_l = 0.02$ ensemble for the APE (upper plots) and HYP data sets (lower plots). The central value

and statistical error of each data point in Fig. 1 are computed as functions of the primary observables $\mathcal{C}^{\mathrm{LW}}$ and $\mathcal{C}^{\mathrm{WW}}$. Then the value of the plateau and its error are computed using a function which averages the values of $m_{B_q}^*$ (or $\Phi_{B_q}^{\mathrm{ren}}$) on time-slices 12, 13, 14, and 15 because we do not observe excited-state contamination in this region. In order to reduce the size of the statistical errors, we average the correlators beginning at two time sources. We achieve the averaging of our two sources by replacing e.g. $\mathcal{C}^{\mathrm{LW}}(t, 0)$ with $[\mathcal{C}^{\mathrm{LW}}(t, 0) + \mathcal{C}^{\mathrm{LW}}(20a - t, 20a)]/2$ in Eqs. (63)–(65). For the case of the HYP-smeared data, these are located at $t/a = 0$ and $t/a = 20$, whereas for the APE-smeared data the second source is located either at $t/a = 20$, 21, or 24.

Finally, we compute the ratio $\Phi_{B_s}^{\mathrm{ren}}/\Phi_{B_l}^{\mathrm{ren}}$ on each ensemble as a function of $\Phi_{B_s}^{\mathrm{ren}}$ and $\Phi_{B_l}^{\mathrm{ren}}$, which themselves
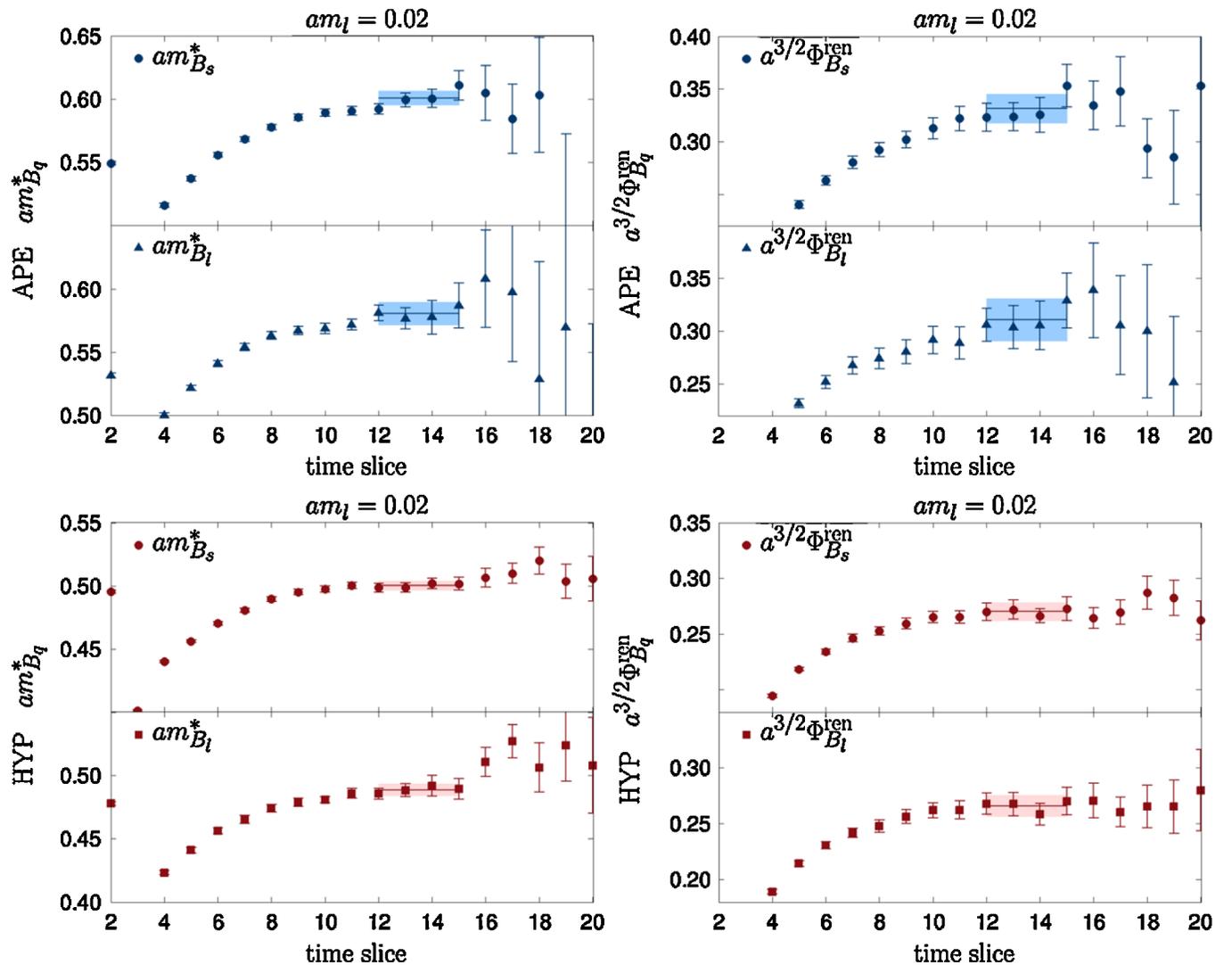

FIG. 1 (color online). Determination of $m_{B_q}^*$ (left) and $\Phi_{B_q}^{\mathrm{ren}}$ (right) using the average of two time sources on the $am_l = 0.02$ ensemble. The upper plots show the APE data, while the lower plots show the HYP-smeared data. For each panel, the shaded band corresponds to the plateau extracted from averaging the data over four consecutive time slices. Errors shown are statistical only.

depend on the corresponding primary observables $\mathcal{C}^{\text{LW}}$ and $\mathcal{C}^{\text{WW}}$; this is shown in Fig. 2. We obtain the plateau for the ratio from time slices 12–15, where we do not observe excited-state contamination in the numerator $\Phi_{B_s}^{\text{ren}}$ or the denominator $\Phi_{B_l}^{\text{ren}}$. Table V presents the values of $\Phi_{B_s}^{\text{ren}}/\Phi_{B_l}^{\text{ren}}$ on the three sea-quark ensembles. Despite the use of two time sources, the statistical errors in the ratio are as large as 7.5% in case of the data using APE smearing.

B. Calculation of the ratio of *B*-meson mixing matrix elements

The $B_q - \bar{B}_q$ mixing parameter in continuum QCD is defined in terms of the matrix element of the $\Delta B = 2$ four-

TABLE V. The renormalized decay amplitude ratio $\Phi_{B_s}^{\text{ren}}/\Phi_{B_l}^{\text{ren}}$ for both the APE- and HYP-smeared data sets. Errors shown are statistical only.

	$\Phi_{B_s}^{\text{ren}}/\Phi_{B_l}^{\text{ren}}$	
am_l/am_h	APE	HYP
0.01/0.04	1.07(8)	1.10(4)
0.02/0.04	1.06(5)	1.02(3)
0.03/0.04	0.97(4)	0.99(2)

fermion operator via Eqs. (2) and (3). Because the matrix element $\mathcal{M}_q$ behaves as m_{B_q} in the limit of large B_q-meson mass, we calculate the desired matrix element divided by
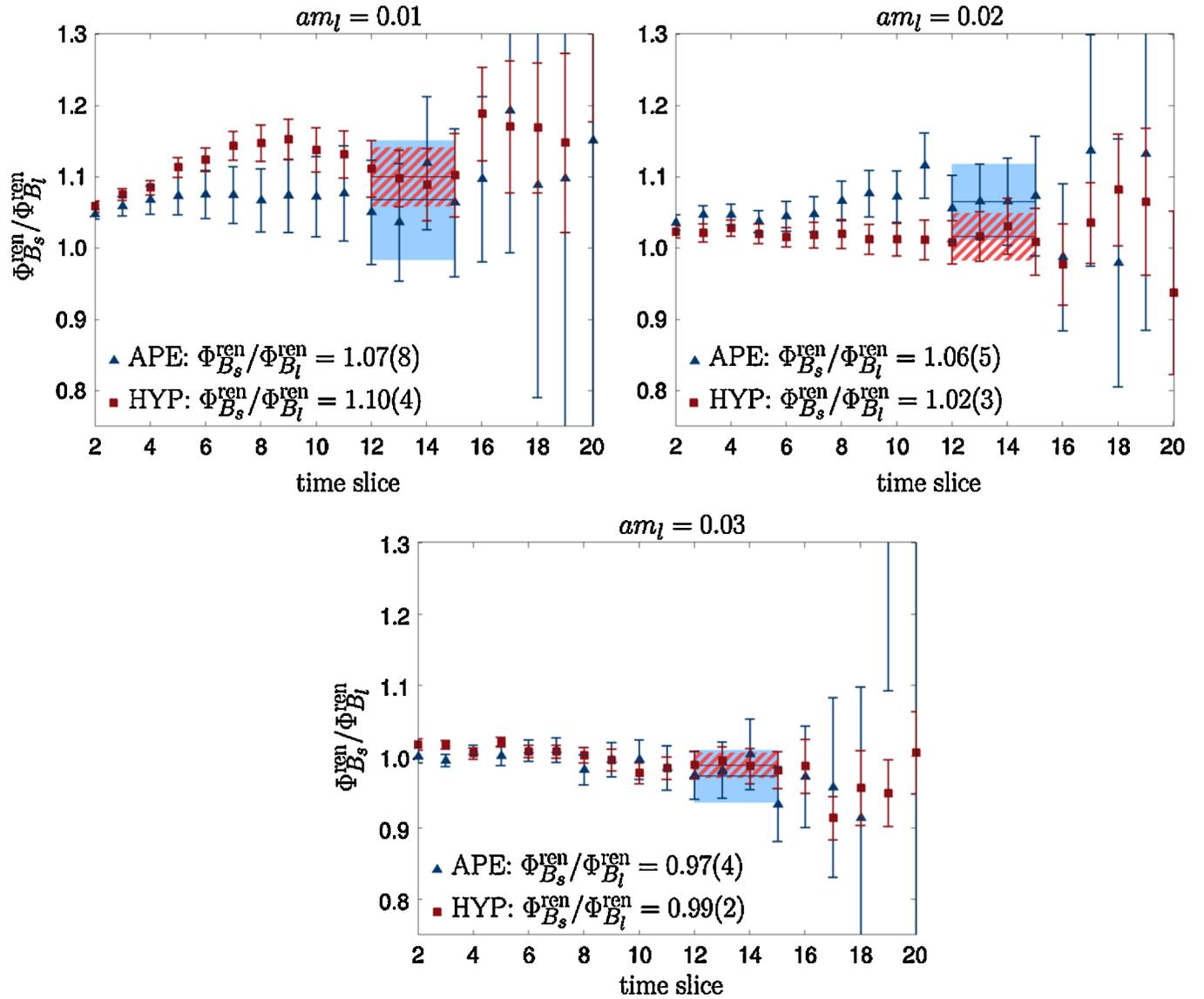

FIG. 2 (color online).   Determination of $\Phi_{B_s}^{\text{ren}}/\Phi_{B_l}^{\text{ren}}$ using the average of two time sources on the three sea quark ensembles. The blue (triangle) points denote the APE data, while the red (square) points denote the HYP-smeared data. The shaded (hatched) band corresponds to the plateau extracted from averaging the APE (HYP) data over four consecutive time slices. Errors shown are statistical only.
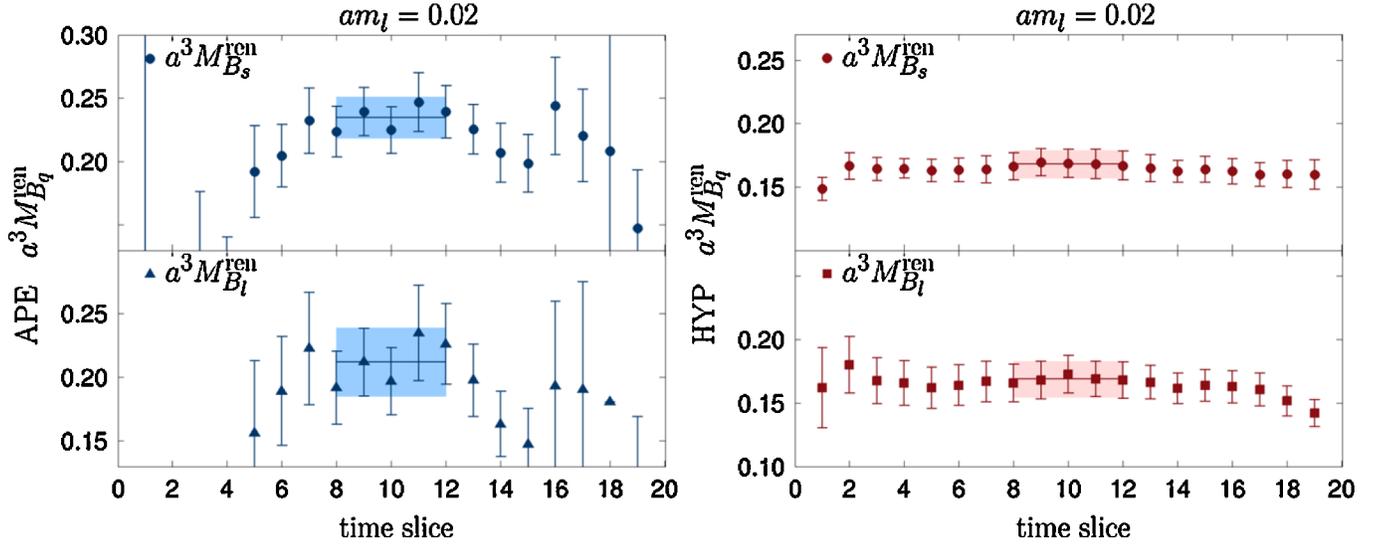
FIG. 3 (color online). Determination of $M_{B_s}^{\rm ren}$ and $M_{B_l}^{\rm ren}$ on the $am_l = 0.02$ ensemble. The left-hand plot shows the APE data, while the right-hand plot shows the HYP-smeared data. For each panel, the shaded band corresponds to the plateau extracted from averaging the data over four consecutive time slices. Errors shown are statistical only.

the B_q-meson mass:

$$M_{B_q} = \mathcal{M}_q / m_{B_q}. \tag{66}$$

For the determination of M_{B_q}, we use different spatial sources for the two choices of link smearing: in the case of APE-smeared links we use box sources of size 8^3, while for HYP smearing we use wall sources. The local-wall two-point functions are already defined in Eq. (59), while the box-box two-point functions are given by

$$\mathcal{C}^{BB}(t, t_0) = \langle 0 | A_0^B(t) A_0^B(t_0)^\dagger | 0 \rangle, \tag{67}$$

with

$$A_0^B(t) = a^6 \sum_{\vec{x}, \vec{y} \in \Delta V} (\bar{h}^{(+)}(\vec{x}, t) \gamma_0 \gamma_5 q(\vec{y}, t)$$
$$+ \bar{h}^{(-)}(\vec{x}, t) \gamma_0 \gamma_5 q(\vec{y}, t)), \tag{68}$$

where the superscript B denotes a box source in the region ΔV. We also compute the three-point correlation functions

$$\mathcal{C}_{O_i}^I(t_f, t, t_0) = a^3 \sum_{\vec{x} \in V} \langle 0 | A_0^{(+)I}(t_f)^\dagger O_i^{\rm lat}(\vec{x}, t) A_0^{(-)I}(t_0)^\dagger | 0 \rangle, \tag{69}$$

where $A_0^{(\pm)I}(t)$ is either the box-source axial current $A_0^{(\pm)B}(t)$ or the wall-source axial current $A_0^{(\pm)W}(t)$. The operator O_i can be either the sum of the squared vector plus squared axial vector current or the squared scalar plus squared pseudoscalar current, respectively,[2]

---

[2] We neglect the odd-parity parts of $O_L^{\rm lat}$ and $O_S^{\rm lat}$, Eqs. (44) and (45), when computing the lattice three-point correlation functions because only the parity-conserving components contribute to the desired matrix element.

$$O_{VV+AA}^{\rm lat} = 2(\bar{h}^{(+)} \gamma^\mu q)(\bar{h}^{(-)} \gamma_\mu q) + 2(\bar{h}^{(+)} \gamma^\mu \gamma_5 q)$$
$$\times (\bar{h}^{(-)} \gamma^\mu \gamma_5 q), \tag{70}$$

$$O_{SS+PP}^{\rm lat} = 2(\bar{h}^{(+)} q)(\bar{h}^{(-)} q) + 2(\bar{h}^{(+)} \gamma_5 q)(\bar{h}^{(-)} \gamma_5 q). \tag{71}$$

Although the $SS + PP$ operator does not contribute to $B_q - \bar{B}_q$ mixing in continuum QCD, its counterpart in HQET is introduced through the QCD $\rightarrow$ HQET matching as shown in Eq. (27).

Because of the different spatial wave functions used for the APE- and HYP-smeared data, we extract the $B_q - \bar{B}_q$ matrix element in different ways for the two data sets. With the APE-smeared box source data, we can compute the matrix element directly from the ratio of correlators [57]

$$M_{O_i} = \lim_{t_f \gg t \gg t_0} 2 \frac{C_{O_i}^B(t_f, t, t_0) e^{m_{B_q}^*(t_f - t_0)/2}}{\sqrt{C^{BB}(t, t_f) C^{BB}(t, t_0)}}. \tag{72}$$

For the HYP-smeared wall-source data, however, we must first extract the bag parameter B_{B_q}

$$B_{O_i} = \lim_{t_f \gg t \gg t_0} \frac{3}{8} L^3 \frac{C_{O_i}^W(t_f, t, t_0)}{C^{LW}(t, t_f) C^{LW}(t, t_0)}, \tag{73}$$

then we obtain the matrix element via

$$M_{O_i} = \frac{8}{3} B_{O_i} (\Phi_{B_q}^{\rm ren})^2. \tag{74}$$

The derivation Eq. (72) is more complex than that of either Eq. (63) or Eq. (73) because the box sources in the amplitudes appearing in both the numerator and denominator are not translationally invariant and will create B-meson states carrying a variety of spatial momenta. As explained in
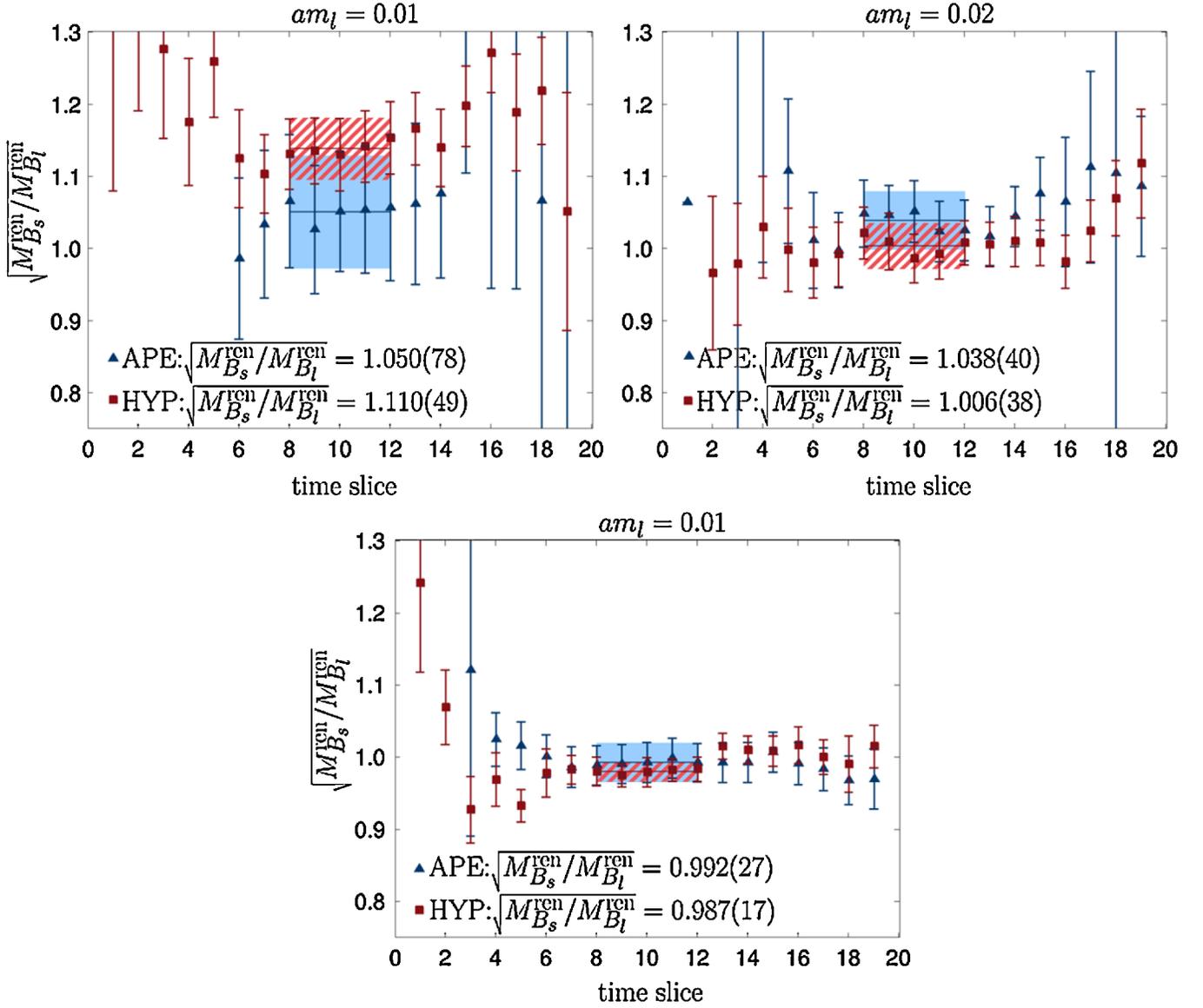
FIG. 4 (color online).   Determination of $\sqrt{M_{B_s}^{\text{ren}}/M_{B_l}^{\text{ren}}}$ using the average of two time sources on the three sea quark ensembles. The blue (triangle) points denote the APE data, while the red (square) points denote the HYP-smeared data. The shaded (hatched) band corresponds to the plateau extracted from averaging the APE (HYP) data over four consecutive time slices. Errors shown are statistical only.

greater detail in Appendix C, these states are degenerate with the lowest energy *B*-meson state and so cannot be suppressed by simply going to large Euclidean time separations. Instead, Eq. (72) is derived in Appendix C using the local conservation of heavy-quark number, a property special to the static approximation. Finally, for both the APE and HYP-smeared data, we compute the renormalized matrix element through $\mathcal{O}(\alpha_s)$,

$$M_{B_q}^{\text{ren}} = Z_{VA}M_{VV+AA}^{\text{lat}} + Z_{SP}M_{SS+PP}^{\text{lat}}, \qquad (75)$$

using the perturbative matching factors given in Table III.

We compute the ratio of mixing matrix elements in the same manner as we compute the ratio of decay constants in the previous subsection. For example, Fig. 3 shows the

determination of the numerator $M_{B_s}^{\text{ren}}$ and the denominator $M_{B_l}^{\text{ren}}$ on the $am_l = 0.02$ ensemble for the APE (left-hand plot) and HYP data sets (right-hand plot). The source

TABLE VI. The renormalized SU(3)-breaking ratio $\sqrt{M_{B_s}^{\text{ren}}/M_{B_l}^{\text{ren}}}$ for both the APE and HYP-smeared data sets. Errors shown are statistical only.

	$\sqrt{M_{B_s}^{\text{ren}}/M_{B_l}^{\text{ren}}}$	
am_l/am_h	APE	HYP
0.01/0.04	1.050(78)	1.110(49)
0.02/0.04	1.038(40)	1.006(38)
0.03/0.04	0.992(27)	0.987(17)

location for the three-point correlators is at time slice 0 and the sink is at time slice 20. We compute the values of the plateaux using time-slices 8–12 because it is at the midpoint between the B_q^0 and $\bar{B}_q^0$ mesons and our result is constant within errors over this region. Although we would prefer to use a region farther separated from the two sources as we have done when determining Φ_{B_l} and Φ_{B_s}, this is not possible given the 20 time unit separation between our two sources. Given, however, that there is no observable excited-state contamination in the three-point correlators, we expect that any resulting systematic uncertainty is negligible as compared to our large statistical and other errors. We will, of course, need to use a larger source-sink separation in our future work when the statistical errors are reduced. Table VI shows the results for the SU(3)-breaking ratios $\sqrt{M_{B_s}^{\mathrm{ren}}/M_{B_l}^{\mathrm{ren}}}$ on the three sea quark ensembles; the corresponding plateau plots are shown in Fig. 4.

V. CHIRAL EXTRAPOLATION

We extrapolate our results for the ratio of the decay constants and for the ratio of mixing matrix elements to the physical point using a phenomenologically-motivated function based on next-to-leading order partially quenched SU(2) heavy-light meson chiral perturbation theory. In SU(2) χPT, the pesudoscalar mesons containing strange quarks (i.e. kaons and η's) are integrated out of the theory. Thus SU(2) χPT does not require an expansion in the strange quark mass about the chiral limit, and the SU(2) χPT expansion parameter in isospin-symmetric simulations is m_l/Λ_χ, where m_l is the light up-down sea quark mass and Λ_χ is a typical hadronic scale. This improves the convergence of the chiral expansion relative to SU(3) χPT, as long as m_l is sufficiently light that corrections of $\mathcal{O}(m_l/m_s)$ are small. Studies by the RBC and UKQCD Collaborations, the PACS-CS Collaboration, and the MILC Collaboration confirm this picture and show that, for light pseudoscalar meson masses and decay constants, SU(2) χPT within its applicable region converges more quickly than SU(3) χPT [34–37]. For the case of SU(3)-breaking ratios such as f_{B_s}/f_{B_d} and ξ, however, SU(3) HMχPT has the advantage that the chiral extrapolation formulas manifestly preserve the fact that the ratios must be equal to one in the limit $m_l \rightarrow m_s$. Within the framework of SU(2) HMχPT, this fact must be introduced in a more *ad hoc* manner such as by matching the SU(2) HMχPT expression at small quark masses onto an analytic form at large quark masses that becomes one when $m_l \rightarrow m_s$. We therefore plan to perform a study comparing the use of SU(2) versus SU(3) HMχPT for the extrapolation of *B*-meson decay constants and mixing matrix elements to the physical quark masses in a future analysis when we have lighter data with smaller statistical errors in order to see which procedure leads to a more accurate determination of these quantities.

Although we know that HMχPT is the correct low-energy effective description of the lattice theory when the simulated quark masses are sufficiently light, we do not know *a priori* at what mass the range of validity of HMχPT ends. Studies of the light pseudoscalar meson sector on the RBC/UKQCD domain-wall ensembles show that NLO χPT does not describe the numerical data for the masses and decay constants when the pion masses are above about 420 MeV [34]. Since the lightest pion mass in our analysis is approximately 430 MeV, this suggests that most of our data may be too heavy for NLO HMχPT to apply and that the inclusion of NNLO terms may be necessary. Unfortunately, because we only have three data points for each of the SU(3)-breaking ratios, we do not have enough data points to reliably constrain the values of the higher-order terms (there are two free parameters at NNLO in the SU(3) HMχPT expressions, and even more at NNLO in SU(2) HMχPT). When the masses of the light pseudoscalar mesons in the chiral logarithms are sufficiently heavy, however, the logarithms can be well approximated by polynomials. We, therefore, choose to fit the data to a linear fit function that is constrained to be equal to one in the SU(3) limit ($m_l \rightarrow m_s$) and then match this result onto the NLO SU(2) HMχPT expression at the location of our lightest data point ($am_l = 0.01$), which we believe is sufficiently light that NLO SU(2) HMχPT should apply. This phenomenologically-motivated matching procedure has been used to extrapolate heavy lattice data by several groups [62–64], but it should not, of course, be used once the pion masses are within the chiral regime.

Although the behavior of the data is unlikely to be strictly linear even in the heavy-mass region, the statistical errors in our data points are sufficiently large (as great as ~8%) that we can successfully perform a linear fit and obtain a good χ^2/dof without the addition of higher-order polynomial terms.[3] Furthermore, we cannot reliably determine the size of a quadratic term if we include one in the fit. Given our poor statistical errors, however, we cannot exclude the possibility of other fit functions, and we use alternate fit forms as one way to estimate the chiral extrapolation error. We also vary the location of the SU(2) HMχPT matching point and the parameters that enter the SU(2) HMχPT expressions, and consider matching onto SU(3) HMχPT. All of these variations are discussed in greater detail when we estimate the systematic uncertainty due to the chiral extrapolation in Sec. VI A.

In the case of the decay constants, we extrapolate the ratio

---

[3]Because the data points for the SU(3)-breaking ratios in Tables V and VI were generated on three different sea-quark ensembles, they are statistically independent; thus the uncorrelated χ^2/dof correctly reflects the goodness-of-fit.

$$\frac{\Phi_{B_s}^{\mathrm{ren}}}{\Phi_{B_l}^{\mathrm{ren}}} = \sqrt{\frac{m_{B_s}}{m_{B_l}}}\frac{f_{B_s}}{f_{B_l}}, \tag{76}$$

while for the mixing matrix elements we consider

$$\sqrt{\frac{M_{B_s}^{\mathrm{ren}}}{M_{B_l}^{\mathrm{ren}}}} = \sqrt{\frac{m_{B_s}}{m_{B_l}}}\left(\frac{f_{B_s}\sqrt{B_{B_s}}}{f_{B_l}\sqrt{B_{B_l}}}\right). \tag{77}$$

From here on, we drop the superscript "ren" for simplicity because we only refer to the renormalized quantities. The expressions for the heavy-light meson decay constant and mixing matrix element to NLO in the light-quark expansion, but zeroth order in $1/m_b$, are given in Appendix D. For completeness, we present formulas for both SU(3) and SU(2) HMχPT. The SU(3) fit functions depend on the valence and sea light-quark masses (m_s, m_l, m_h) and the lattice spacing a. The SU(2) functions are obtained from the SU(3) expressions by taking the limit $(\frac{m_l}{m_s}, \frac{m_l}{m_h}) \ll 1$. Thus they only apply in the region in which the value of the average up-down quark mass is much smaller than the valence and sea strange quark masses. Furthermore, because the strange quark has been integrated out of the SU(2) theory, the SU(2) fit functions only depend upon the light-quark mass m_l and the lattice spacing a. Therefore, the expressions for the SU(3)-breaking ratios at NLO in SU(2) HMχPT are particularly simple:

$$\frac{\Phi_{B_s}}{\Phi_{B_l}} = R_\Phi\left\{1 + \frac{1 + 3g_{B^*B\pi}^2}{(4\pi f)^2}\left(\frac{3}{4}\right)m_L^2 \ln\left(\frac{m_L^2}{\Lambda_\chi^2}\right)\right.$$
$$\left. + C_l\frac{2Bm_l}{(4\pi f)^2}\right\}, \tag{78}$$

$$\sqrt{\frac{M_{B_s}}{M_{B_l}}} = R_M\left\{1 + \frac{2 + 3g_{B^*B\pi}^2}{(4\pi f)^2}\left(\frac{1}{2}\right)m_L^2 \ln\left(\frac{m_L^2}{\Lambda_\chi^2}\right)\right.$$
$$\left. + D_l\frac{Bm_l}{(4\pi f)^2}\right\}, \tag{79}$$

where $m_L^2 = 2B(m_l + m_{\mathrm{res}})$ is the tree-level mass-squared of a pseudoscalar meson composed of two quarks with mass m_l, B, and f are the leading-order low-energy constants of χPT, and the quark masses in the analytic terms are expressed in terms of dimensionless ratios to make the coefficients C_l and D_l of $\mathcal{O}(1)$. These functional forms are derived from Eqs. (D16)–(D20) by taking the ratio of the expressions for the valence quark $y = s$ over the expressions for $x = l$. Because we are working at a single lattice spacing, the analytic terms proportional to a^2 are absorbed into the values of the leading-order coefficients R_Φ and R_M. Note that in the limit $m_l \to m_s$ the SU(3)-breaking ratios are not constrained to unity, as would be the case in SU(3) HMχPT. (In fact, the point $m_l = m_s$ does not even lie within the range of validity of SU(2) HMχPT and hence of Eqs. (78) and (79).) This is because, once the strange quark has been integrated out of the SU(2) theory, the expressions no longer contain explicit strange-quark mass dependence. All of the effects of the strange quark are encoded in the values of the low-energy constants, which differ in the SU(2) and SU(3) theories.

Although the coefficients of the chiral logarithms depend on the low-energy constants $g_{B^*B\pi}$, f, and B, once these are fixed as we now describe, there are only two free parameters each in Eqs. (78) and (79): the overall normalization and the coefficient of the analytic term proportional to m_l. This allows us to smoothly match the SU(2) expressions onto the linear fit of the heavy data without ambiguity. In the chiral extrapolation we obtain our central value using $g_{B^*B\pi} = 0.516$ for the B^*-B-π coupling, which comes from a two-flavor lattice determination in the static heavy quark limit by Ohki, Matsufuru, and Onogi [65]. We then vary the value of $g_{B^*B\pi}$ over a reasonable spread of values based on both lattice calculations and phenomenological fits to experimental data in order to estimate the systematic uncertainty, as described in further detail in Sec. VI B. Moreover, we set the leading-order pseudoscalar meson decay constant f to the experimental value of $f_\pi = 130.4 \pm 0.04 \pm 0.2$ MeV [6]. This is consistent to the order in χPT at which we are working since it only modifies higher-order NNLO terms. Studies by both the MILC and JLQCD Collaborations suggest that the use of a physical parameter in the chiral coupling $(f \to f_\pi)$ leads to improved convergence of χPT [66,67]. The scale in the chiral logarithms is fixed by setting $\Lambda_\chi = 1$ GeV. For the low-energy constant B we use the value $aB = 2.414(61)$ obtained from a NLO fit of the pseudoscalar meson masses [34]. Finally, whenever the residual quark mass appears, we use its value in the chiral limit $am_{\mathrm{res}} = 0.003\,15$.

The results of the chiral extrapolation are shown in Figs. 5 and 6. The blue triangles (red squares) show the data obtained using APE (HYP) link smearing and are plotted versus the light sea quark mass. We indicate the location of the physical strange quark mass m_s by the black dot. The dashed vertical line marks the physical average u-d quark mass, which is the point at which we extract the physical values for Φ_{B_s}/Φ_{B_d} and $\sqrt{m_{B_s}/m_{B_d}}\xi$. The agreement between the two smearings is good. For the case of the APE data, the χ^2/dof for the fit of both SU(3)-breaking ratios is below one, indicating that the data are well-described by the linear fit function. For the HYP data, the χ^2/dof's are 1.8 for Φ_{B_s}/Φ_{B_d} and 2.0 for $\sqrt{m_{B_s}/m_{B_d}}\xi$, respectively. These still correspond to confidence levels of greater than 10%, however, and are therefore consistent with the data. The error bands in Figs. 5 and 6 are fairly broad and hence the statistical uncertainty at the physical point is large, $\sim4.1\%$–7.6% for Φ_{B_s}/Φ_{B_d} and $\sim4.7\%$–6.3% for $\sqrt{m_{B_s}/m_{B_d}}\xi$. This is due to the large statistical errors in our data points, as well as the fact that our lightest mass is still quite heavy, which forces us to extrapolate over a large mass range.
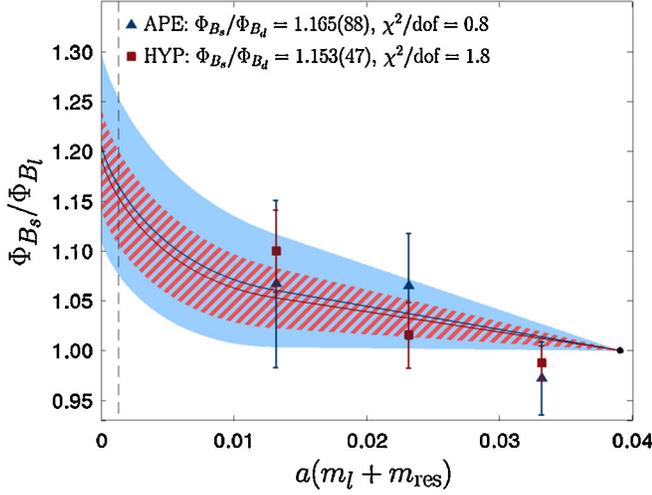
FIG. 5 (color online). Chiral extrapolation of $\Phi_{B_s}/\Phi_{B_l} = \sqrt{m_{B_s}/m_{B_l}} \cdot f_{B_s}/f_{B_l}$. The blue (triangle) points denote the APE data, while the red (square) points denote the HYP-smeared data. The color of the shaded (hatched) error band corresponds to those of the APE (HYP) data points. The dashed vertical line denotes the physical average *u-d* quark mass and the black dot denotes the physical strange quark mass, at which the SU(3)-breaking ratio must be one. The SU(2) HMχPT coefficients obtained from the fit are $R_\Phi = 1.21(9)$ and $C_l = 1.1(6)$ in the case of APE smearing and $R_\Phi = 1.19(5)$ and $C_l = 1.2(3)$ in the case of HYP smearing. Errors shown are statistical only.
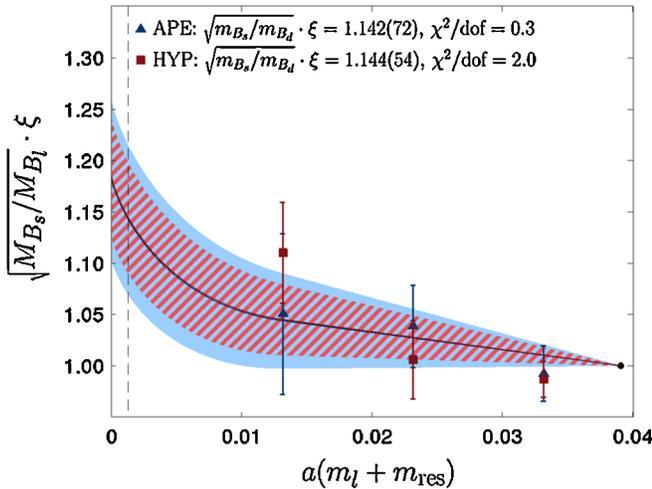
FIG. 6 (color online). Chiral extrapolation of $\sqrt{M_{B_s}/M_{B_l}} = \sqrt{m_{B_s}/m_{B_l}}(f_{B_s}\sqrt{B_{B_s}}/f_{B_l}\sqrt{B_{B_l}})$. The blue (triangle) points denote the APE data, while the red (square) points denote the HYP-smeared data. The color of the shaded (hatched) error band corresponds to those of the APE (HYP) data points. The dashed vertical line denotes the physical average *u-d* quark mass and the black dot denotes the physical strange quark mass, at which the SU(3)-breaking ratio must be one. The SU(2) HMχPT coefficients obtained from the fit are $R_M = 1.18(8)$ and $D_l = 2.6(1.1)$ in the case of APE smearing and $R_M = 1.18(6)$ and $D_l = 2.6(8)$ in the case of HYP smearing. Errors shown are statistical only.

TABLE VII. Results for Φ_{B_s}/Φ_{B_d} and $\sqrt{m_{B_s}/m_{B_d}} \cdot \xi$ at the physical point. Only statistical errors are shown.

	Link smearing	
	APE	HYP
Φ_{B_s}/Φ_{B_d}	1.165(88)	1.153(47)
$\sqrt{m_{B_s}/m_{B_d}} \cdot \xi$	1.142(72)	1.144(54)

We should emphasize that the chiral extrapolation procedure used here (the combination of a linear fit matched onto the predictions of NLO SU(2) HMχPT) is appropriate only for the present case when the available light quark masses are quite heavy. In future calculations with more physical light quark masses we will perform a fit directly to the NLO SU(2) HMχPT formulas in Eqs. (78) and (79). We will also examine a possible NLO SU(3) HMχPT fit in order to exploit the known, unit values of these ratios at the SU(3) symmetric point. Of course, high priority will be given to calculations performed with physical light quark masses so that such difficulties can be avoided. We summarize the results of our current preferred chiral extrapolation in Table VII and discuss the estimation of our systematic errors in the following section.

VI. ESTIMATION OF SYSTEMATIC ERRORS

In this section we estimate the systematic uncertainties in the SU(3)-breaking ratios f_{B_s}/f_{B_d} and ξ. For clarity, we present each source of error in a separate subsection. The total error budgets for both quantities are given at the end of the section in Table VIII.

A. Chiral extrapolation fit ansatz

As described in the previous section, we extrapolate our data to the physical quark masses using a linear fit matched onto NLO SU(2) HMχPT at the value of our lightest data point. The SU(2) expressions are derived using the symmetries of the lattice theory; therefore, they contain the

TABLE VIII. Total error budget for the SU(3)-breaking ratios f_{B_s}/f_{B_d} and ξ. Each source of uncertainty is discussed in Sec. VI, and is rounded to the nearest percentage.

	f_{B_s}/f_{B_d}		ξ	
Uncertainty	APE	HYP	APE	HYP
Statistics	8%	4%	6%	5%
Chiral extrapolation	7%	7%	7%	7%
Uncertainty in $g_{B^*B\pi}$	3%	3%	2%	2%
Discretization error	3%	3%	4%	4%
Renormalization factors	0%	0%	2%	2%
Scale and quark mass uncertainties	1%	1%	1%	1%
Finite volume error	1%	1%	1%	1%
$1/m_b$ corrections	2%	2%	2%	2%
Total systematics	9%	9%	9%	9%

correct dependence of the B-meson decay constants and mixing matrix elements on the quark mass and lattice spacing through NLO when the quark masses are sufficiently light. Given the large light-quark masses used in our simulations; however, it may be that the SU(2) chiral logarithms do not become important until the pion mass is even lighter than the range of our data. Thus we vary the location of the matching point as one way to estimate the systematic uncertainty due to the chiral extrapolation. In addition, because we use NLO SU(2) HMχPT to obtain our central value, we must estimate the systematic uncertainty due to the truncation of higher-orders in HMχPT. We do this in several ways: (i) by explicitly adding higher-order terms to the linear plus SU(2) HMχPT fit function, (ii) by matching the linear fit onto the NLO SU(3) HMχPT expressions, and (iii) by varying the value of the low-energy constant f in the coefficient of the NLO chiral logarithms.

Because we do not know *a priori* at what mass the SU(2) chiral logarithms become important, we vary the point at which we match the linear fit onto NLO SU(2) HMχPT in order to estimate the systematic uncertainty due to the choice of matching point. At the matching point used in the preferred fit, the ratio of the light up-down quark mass to the strange valence-quark mass is $am_l/am_s \approx 0.28$ and to the strange sea quark mass is $am_l/am_h = 0.25$. Since both of these quantities are small, we expect the strange quark can be integrated out of the chiral effective theory and that SU(2) HMχPT is applicable in this region. As the light-quark mass decreases, SU(2) becomes an even better approximation. At light-quark masses above this point, however, the ratios am_l/am_s and am_l/am_h are no longer small expansion parameters, and SU(2) will eventually

cease to apply. Therefore, when we estimate the systematic error due to the choice of matching point, we only consider extrapolations in which the matching point is closer to the chiral limit than in the preferred fit. The limiting case is where the matching point is at the chiral limit, which corresponds to a purely linear extrapolation. Although the choice of a linear fit is not based on effective field theory, it cannot be ruled out by the data. We therefore take the difference between the extrapolated values for f_{B_s}/f_{B_d} and ξ obtained with the preferred fit and with a purely linear fit to estimate the systematic error due to the choice of matching point; this leads to an error in f_{B_s}/f_{B_d} of 6.6% for both the APE and HYP data and in ξ of 6.8% (6.9%) for the APE (HYP) data. We compare the results of the preferred fit with those of the purely linear extrapolation in Fig. 7 for Φ_{B_s}/Φ_{B_l} and in Fig. 8 for $\sqrt{m_{B_s}/m_{B_l}}\xi$. Comparison with the linear extrapolation leads to a conservative systematic error estimate since we know that, when the pion mass is sufficiently light, the chiral logarithms will become important and the extrapolation function will begin to curve upward. However, the linear fit provides a clear lower-bound on the possible extrapolated value.

In order to estimate the error due to the omission of higher-order terms in the chiral expansion, we compare the result of the linear plus NLO SU(2) HMχPT fit to a fit supplemented by NNLO analytic terms. Once the valence and sea strange quarks have been integrated out of the chiral effective theory, the SU(2) HMχPT expressions can only depend upon the light up-down quark mass m_l and the lattice spacing a. Thus the only possible NNLO analytic terms are those proportional to m_l^2, $m_l a^2$, and a^4. Because we are working at a single lattice spacing, the
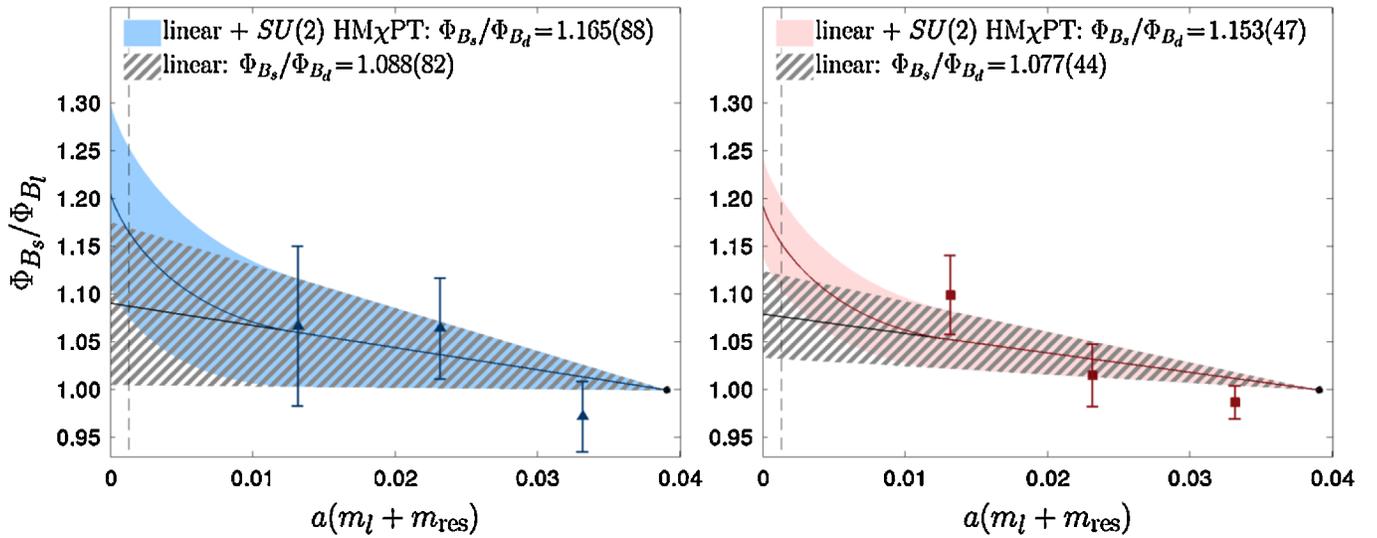

FIG. 7 (color online). Chiral extrapolation of $\Phi_{B_s}/\Phi_{B_l} = \sqrt{m_{B_s}/m_{B_l}} \cdot f_{B_s}/f_{B_l}$ using a linear fit matched onto NLO SU(2) HMχPT at the lightest data point (solid band) and a linear extrapolation all the way to the chiral limit (hatched band). Errors shown are statistical only. The left plot shows the comparison for the APE data, while the right plot shows the same comparison for they HYP-smeared data.
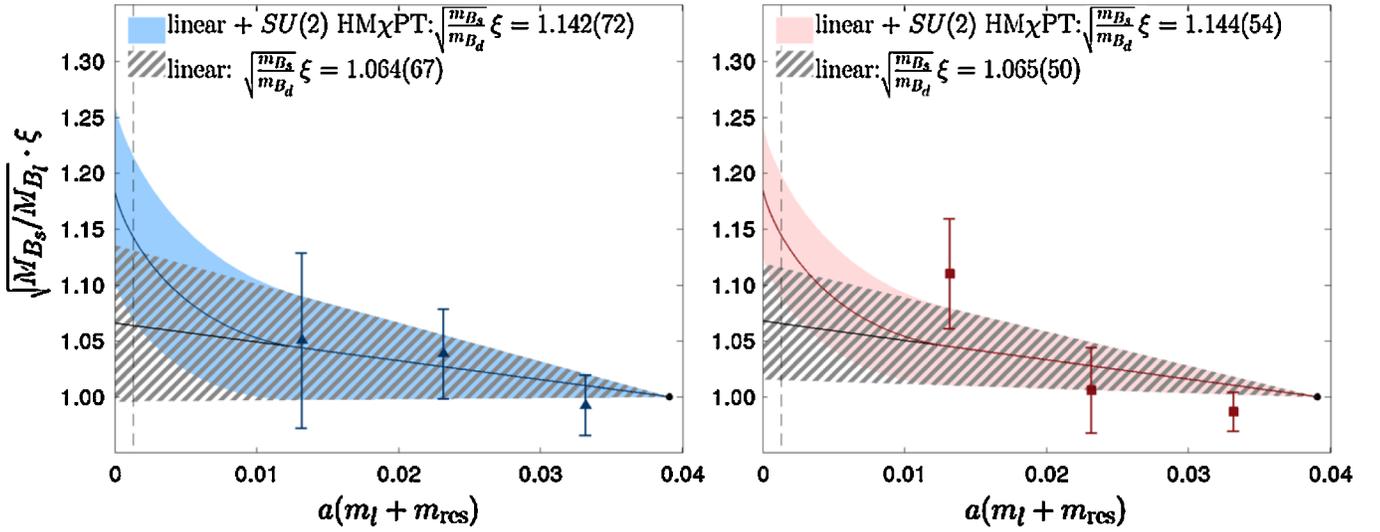
FIG. 8 (color online). Chiral extrapolation of $\sqrt{M_{B_s}/M_{B_l}} = \sqrt{m_{B_s}/m_{B_l}}(f_{B_s}\sqrt{B_{B_s}}/f_{B_l}\sqrt{B_{B_l}})$ using a linear fit matched onto NLO SU(2) HMχPT at the lightest data point (solid band) and a linear extrapolation all the way to the chiral limit (hatched band). Errors shown are statistical only. The left plot shows the comparison for the APE data, while the right plot shows the same comparison for they HYP-smeared data.

contribution proportional to a^4 is indistinguishable from the LO normalization factors R_Φ and R_M in Eqs. (78) and (79) and the contribution proportional to $m_l a^2$ is indistinguishable from the NLO terms $C_l m_l$ and $D_l m_l$. Thus there is only one additional free parameter at NNLO. In practice, we implement the "NNLO fit" by performing a quadratic fit in m_l to our data and then matching to the NLO SU(2) HMχPT expressions supplemented by the NNLO analytic term proportional to m_l^2 at the value of our lightest data point. When we include the term quadratic in m_l, however, the extrapolated values for f_{B_s}/f_{B_d} and ξ have significantly larger statistical errors (about 20%–40%) than those obtained with the preferred fit (about 4–8%). Therefore we cannot draw any meaningful conclusion about the change in the central values of f_{B_s}/f_{B_d} and ξ, since the outcome of the NNLO extrapolation is consistent with the NLO extrapolation within the large statistical errors. This increase in statistical errors is to be expected since we have introduced an extra free parameter, and it is difficult to constrain two parameters with only three data points. Thus we do not use the "NNLO fit" as a way to estimate the chiral extrapolation error in this work, but leave it as a way to estimate the uncertainty due to the omission of higher-order terms in future analyses when we have more data points and smaller statistical errors.

We can also estimate the systematic uncertainty in the chiral extrapolation by comparing the values of f_{B_s}/f_{B_d} and ξ obtained by matching onto SU(2) HMχPT with those obtained by matching onto SU(3) HMχPT. Although the SU(2) chiral logarithms are a subset of the SU(3) chiral logarithms, the SU(2) and SU(3) theories have different series expansions and different degrees-of-convergence within their ranges of applicability.

Therefore, the comparison with NLO SU(3) HMχPT provides another means of estimating the error due to the use of NLO SU(2) HMχPT. The expressions for SU(3)-breaking ratios at NLO in SU(3) HMχPT are, schematically,

$$\frac{\Phi_{B_s}}{\Phi_{B_l}} = 1 + \text{``chiral logs''} + \frac{2B}{(4\pi f)^2}\tilde{c}_{\text{val}}(m_s - m_l), \quad (80)$$

$$\sqrt{\frac{M_{B_s}}{M_{B_l}}} = 1 + \text{``chiral logs''} + \frac{B}{(4\pi f)^2}\tilde{d}_{\text{val}}(m_s - m_l), \quad (81)$$

where "chiral logs" indicate nonanalytic functions of the pseudo-Goldstone meson masses, e.g. $m_L^2 \log(m_L^2/\Lambda_\chi^2)$. These are derived from Eqs. (D2) and (D3) by taking the ratio of the expressions for the valence quark $x = s$ over the expressions for $x = l$. Because the strange quark is treated in the same manner as the up and down quarks in the SU(3) chiral effective theory, the low-energy constants are the same in the numerator and denominator. Thus the overall normalizations cancel in the expressions in Eqs. (80) and (81) and the ratios are constrained to unity in the limit $m_l \to m_s$. Therefore, the expressions for the SU(3)-breaking ratios have one free parameter each, instead of two as in the SU(2) HMχPT case. This means that the SU(3) HMχPT expressions cannot be matched smoothly onto the linear fit of the heavy data. We choose to make the value of the extrapolation function continuous, while leaving a discontinuity in the slope at the matching point. The difference between the linear plus NLO SU(2) HMχPT fit and the linear plus NLO SU(3) HMχPT fit

leads to a difference in f_{B_s}/f_{B_d} of 2.3% (2.4%) for the APE (HYP) data and in ξ of 2.6% (2.5%) for APE (HYP).

In the preferred linear plus NLO SU(2) HMχPT fit, we set the leading-order pseudoscalar meson decay constant f equal to the experimentally-measured value of f_π. This fixes the coefficient of the chiral logarithms and improves the convergence of the chiral expansion [66,67]. At NLO in χPT, however, it is equally consistent to use the pseudoscalar decay constant in the SU(2) chiral limit f_0 or the kaon decay constant f_K because the different choices only affect NNLO terms that are of higher order than we consider. We therefore vary f between $f_0 = 115$ MeV [34] and $f_K = 155.5$ MeV [6] in order to estimate the systematic uncertainty due to the omission of higher-order terms in the chiral expansion. The use of f_0 in the SU(2) chiral limit, which the RBC and UKQCD Collaborations find to be about 10% lower than f_π, leads to a difference from the central value for f_{B_s}/f_{B_d} of 2.1% (2.2%) for APE (HYP) and from the central value for ξ of 2.3% for both APE and HYP. The use of f_K leads to similar changes in f_{B_s}/f_{B_d} of 2.1% and in ξ of 2.2%.

We take the largest of the uncertainties enumerated above, which is obtained from the difference between the preferred linear plus NLO SU(2) HMχPT fit and the purely linear fit, for the final estimate of the chiral extrapolation error; this leads to the values in the row labeled "chiral extrapolation" in Table VIII.

B. Uncertainty due to $g_{B^*B\pi}$

Although we fix the value of the B^*-B-π coupling (and hence the coefficient of the one-loop chiral logarithms) in the chiral extrapolation of our lattice data, $g_{B^*B\pi}$ is in fact poorly known from phenomenology. Hence we must vary the value of $g_{B^*B\pi}$ over a sensible range based on lattice QCD calculations and phenomenology in order to estimate the systematic errors in f_{B_s}/f_{B_d} and ξ due to the uncertainty in the coefficient of the one-loop chiral logarithms.

There has only been one unquenched lattice QCD calculation of the B^*-B-π coupling with a complete associated error budget, which gives $g_{B^*B\pi} = 0.516(5)(50)$, where the first uncertainty is statistical and the second is systematic [65]. Although this value was computed in the static heavy-quark limit and neglects the effects of the dynamical strange quark, we take this as our central value because of its small statistical errors and full systematic error budget, as well as because it lies in the middle of the range of values presented in the literature. Another recent determination of $g_{B^*B\pi} = 0.44 \pm 0.03^{+0.07}_{-0.00}$ in the static limit in two-flavor lattice QCD, where the errors are due to statistics and the chiral extrapolation uncertainty, is consistent with this result [68]. QCD sum rules and the relativistic quark model give a slightly lower value of $g_{B^*B\pi} \approx 0.38 \pm 0.08$ [69]. The value of the B^*-B-π coupling is expected to be close to the D^*-D-π coupling because of heavy-quark symmetry. We can therefore also

use lattice QCD calculations and phenomenological extractions of $g_{D^*D\pi}$ as estimates. Bećirević and Haas recently computed $g_{D^*D\pi} = 0.71(7)$ in 2-flavor lattice QCD, but this result is from only a single lattice spacing and presents no estimate of the systematic error [70]. Stewart computed the value of $g_{D^*D\pi}$ in 1998 by fitting to experimental data [71], and recently updated his result to include the experimental measurement of the D^* decay width [72]. His latest determination is $g_{D^*D\pi} = 0.51$, but with no error quoted [73]. The most sophisticated extraction of the D^*-D-π coupling was performed by Kamenik and Fajfer, and gives $g_{D^*D\pi} = 0.66^{+0.08}_{-0.06}$, where the uncertainty only reflects the error due to counterterms [74]. Finally, we note that the chiral-continuum extrapolations of B-meson quantities by the Fermilab/MILC Collaboration [75] and the HPQCD Collaboration [14] tend to prefer even smaller values of the B^*-B-π coupling than those in the literature.

Most of the results presented above do not have complete error budgets, and are inconsistent within the quoted errors, so for this work we take $g_{B^*B\pi} = 0.516 \pm 0.2$ to account for the spread of values. We then vary $g_{B^*B\pi}$ within this range to determine how much it changes the central values for f_{B_s}/f_{B_d} and ξ. This leads to an uncertainty in f_{B_s}/f_{B_d} of 3.2% for both APE and HYP and in ξ of 2.1%.

C. Discretization errors

In this work we only analyze data at a single, relatively coarse lattice spacing of $a \approx 0.11$ fm, so we estimate the size of discretization errors with power counting. As a consistency check of our estimation procedure, however, we can compare the estimated errors in the individual decay constants and matrix elements with the observed differences in those quantities for the APE and HYP-smeared data. This is because, aside from statistical errors, the differences in the values obtained from the two smearings are due to discretization effects and higher order corrections to the renormalization factors. We find about 15%–20% differences in the decay constants and matrix elements obtained from the APE and HYP-smeared data, whereas we estimate by power counting that discretization errors in f_{B_q} should be about 15% and in $\mathcal{M}_q$ should be about 20%. Thus our observations are consistent with the scaling behavior expected from power counting. We can also compare our power-counting estimates with the findings of the ALPHA Collaboration, who performed a study of f_{B_s} at several lattice spacings using static b-quarks with similar link smearings in the quenched approximation [76]. Although ALPHA observes a violation of $\mathcal{O}(a^2)$ scaling behavior at inverse lattice spacings below $a^{-1} \approx 2.5$ GeV, the difference between the predicted value for f_{B_s} at $a \approx 0.11$ fm given $\mathcal{O}(a^2)$ scaling and the value of f_{B_s} that they obtain in the continuum limit using data within the scaling region is only about 25%, which is again close to our power-counting estimate. Thus we expect that naive

power-counting should lead to a reasonable estimate of the discretization error in the SU(3)-breaking ratios.

For the error estimates in this subsection, we evaluate the strong coupling constant at the lattice scale, $\alpha_s^{\overline{\rm MS}}(1/a) \sim 1/3$. We choose $\Lambda_{\rm QCD} = 500$ MeV because the typical QCD scale that enters heavy-light quantities tends to be larger than for light-light quantities, as indicated by fits to moments of inclusive *B*-decays using the heavy-quark expansion [77]. Fortunately, some of the finite lattice-spacing effects cancel in the ratios f_{B_s}/f_{B_d} and ξ. This can be seen by the fact that, although the APE and HYP data differ by about 15%–20% for the individual decay constants and matrix elements, they agree within statistical errors for the ratios. In SU(3)-breaking quantities, errors must be proportional to the difference in quark masses $(m_s - m_d)$. Dimensional analysis therefore suggests that contributions to the total discretization error are suppressed by the factor $(\tilde{m}_s - \tilde{m}_d)/\Lambda_{\rm QCD} \sim 1/5$, where we use $\tilde{m}_s$ and $\tilde{m}_d$ to denote the renormalized quark masses in the $\overline{\rm MS}$ scheme [6] (as opposed to the bare lattice quark masses) in this subsection and the next. The observed size of SU(3)-breaking effects in the *B*-meson decay constants $(f_{B_s}/f_{B_d} - 1)$ and in the *B*-mixing matrix elements $(\xi - 1)$ are consistent with this expectation. Discretization errors in f_{B_s}/f_{B_d} and ξ can arise from both the actions and the operators. We estimate each source of error separately, and add them in quadrature to obtain the total discretization error.

None of the actions that we are using are $\mathcal{O}(a^2)$-improved. Therefore, the leading discretization errors from the domain-wall fermion action and Iwasaki gauge action are of $\mathcal{O}(a^2\Lambda_{\rm QCD}^2)$. When combined with the SU(3)-breaking suppression factor, this leads to discretization errors in the ratios f_{B_s}/f_{B_d} and ξ of $\mathcal{O}(a^2\Lambda_{\rm QCD}^2 \times (\tilde{m}_s - \tilde{m}_d)/\Lambda_{\rm QCD}) \sim 1.7\%$. The leading heavy-quark discretization errors from the static action are also of $\mathcal{O}(a^2\Lambda_{\rm QCD}^2)$. Hence heavy-quark discretization errors also contribute $\sim 1.7\%$ to the total error in the ratios. Because we improve the heavy-light axial current used to compute the decay constant through $\mathcal{O}(\alpha_s ap)$, the leading discretization errors from the heavy-light current are of $\mathcal{O}(\alpha_s am)$, $\mathcal{O}(\alpha_s^2 a\Lambda_{\rm QCD})$, and $\mathcal{O}(a^2\Lambda_{\rm QCD}^2)$.[4] When combined with the SU(3)-breaking suppression factor, this leads to discretization errors in the ratio f_{B_s}/f_{B_d} of $\mathcal{O}(\alpha_s \times (am_s - am_d)) \sim 1.2\%$ plus $\mathcal{O}(\alpha_s^2 a\Lambda_{\rm QCD} \times (\tilde{m}_s - \tilde{m}_d)/\Lambda_{\rm QCD}) \sim 0.6\%$ plus $\mathcal{O}(a^2\Lambda_{\rm QCD}^2 \times (\tilde{m}_s - \tilde{m}_d)/\Lambda_{\rm QCD}) \sim 1.7\%$. Although we do not improve the heavy-light four-fermion operator used to compute the *B*-mixing matrix element, the operator

---

[4]There are also discretization errors from mixing with operators of other chiralities that are proportional to $am_{\rm res}$. These effects, however, are expected to be sub-percent level in the matrix elements [78], and, therefore, negligible in the SU(3)-breaking ratios.

does not have any tree-level $\mathcal{O}(a)$ errors [38]. Thus the leading discretization errors in the ratio ξ from the four-fermion operator are of $\mathcal{O}(\alpha_s \times (am_s - am_d)) \sim 1.2\%$ plus $\mathcal{O}(\alpha_s a\Lambda_{\rm QCD} \times (\tilde{m}_s - \tilde{m}_d)/\Lambda_{\rm QCD}) \sim 1.9\%$ plus $\mathcal{O}(a^2\Lambda_{\rm QCD}^2 \times (\tilde{m}_s - \tilde{m}_d)/\Lambda_{\rm QCD}) \sim 1.7\%$.

Adding the contributions from light-quark and gluon discretization errors, heavy-quark discretization errors, and discretization errors in the heavy-light current or four-fermion operator in quadrature, we estimate the error in f_{B_s}/f_{B_d} to be $\sim 3.2\%$ and the error in ξ to be $\sim 3.7\%$.

D. Heavy-light current and four-fermion operator renormalization

We compute the renormalization factors needed to match the lattice axial current and four-fermion operator to the continuum using one-loop lattice perturbation theory. This leaves a residual error due to the omission of higher-order terms. Based on power counting, we estimate the truncation error in the coefficients to be of $\mathcal{O}(\alpha_s^2)$, which is the size of the first neglected term in the series. As we noted earlier in Sec. III C, however, the matching coefficient Z_Φ cancels in the ratio of decay constants f_{B_s}/f_{B_d}; thus its contribution to the error in f_{B_s}/f_{B_d} is zero. Although such an exact cancellation does not occur for the ratio of mixing matrix elements ξ, the error in ξ due to the uncertainty in the ratio of matching coefficients Z_{SP}/Z_{VA} is suppressed by the SU(3)-breaking factor $(\tilde{m}_s - \tilde{m}_d)/\Lambda_{\rm QCD}$. This is because, in the SU(3) limit, the four-fermion operator matrix elements would be equal in the numerator and denominator, so the error in ξ from the renormalization factor uncertainty would be zero. We therefore expect the error in f_{B_s}/f_{B_d} to be 0% and the error in ξ to be of $\mathcal{O}(\alpha_s^2 \times (\tilde{m}_s - \tilde{m}_d)/\Lambda_{\rm QCD}) \sim 2.2\%$. This error will decrease with the inclusion of data at a finer lattice spacing because the smaller coupling constant will improve the convergence of the series.

E. Scale uncertainty

Because in this paper we only compute dimensionless ratios, the uncertainty in the determination of the lattice spacing only enters implicitly through the uncertainty in the light-quark masses and in the renormalization factors. We estimate the systematic error due to the truncation of lattice perturbation theory in the previous subsection and due to the light-quark mass determinations in the following subsection.

F. Light- and strange-quark mass uncertainties

We obtain the physical decay constants and mixing matrix elements by setting the light-quark masses to their physical values in the linear plus SU(2) HMχPT chiral extrapolation formulas, once the low-energy constants have been determined from fits to numerical lattice data. We use the bare-quark mass value determined from fits to

the light pseudoscalar meson masses [34]:

$$am_{ud} + am_{\mathrm{res}} = 0.001\,300(85), \qquad (82)$$

where m_{ud} is the average of the up and down quark masses. The quoted error includes both statistics and the systematic uncertainties from the chiral extrapolation, finite-volume effects, discretization effects, and the unphysical strange sea quark mass. In order to estimate the systematic uncertainty in the ratios f_{B_s}/f_{B_d} and ξ, we vary the bare light-quark masses within their stated uncertainties. We then take the maximal difference from the central value to be the systematic error. From this method, we find that the systematic error in f_{B_s}/f_{B_d} due to the uncertainty in the light-quark mass determination is 0.2% for both smearings and the systematic error in ξ is 0.2% regardless of the smearing used for the heavy quark.

Because the strange-quark mass does not explicitly appear in the SU(2) HMχPT extrapolation formulas, we cannot estimate the errors in f_{B_s}/f_{B_d} and ξ due to the simulated valence and sea strange-quark masses with the simple method used above for the light quarks. We must instead address the errors due to the uncertainty in the strange valence-quark mass (which is set to the physical value of m_s) separately from those due to the choice of strange sea-quark mass (which is not tuned to the physical m_s).

We calculate the decay constants and mixing matrix elements with the strange valence-quark mass tuned to the physical value obtained from fits of the light pseudoscalar meson masses [19]:

$$am_s + am_{\mathrm{res}} = 0.0390(21), \qquad (83)$$

where the error includes those due to statistics and to uncertainties in the pseudoscalar meson masses, residual mass, and lattice scale. Since the time at which our numerical computation was performed, however, we have improved the strange-quark mass determination using data on the larger-volume 24^3 ensemble. This analysis yields $am_s + am_{\mathrm{res}} = 0.0375(17)$ [34], where the error includes statistics and the systematic uncertainties from the chiral extrapolation, finite-volume effects, discretization effects, and the unphysical strange sea quark mass. Fortunately, the two determinations are consistent within their stated uncertainties and the small change in valence strange-quark mass leads to a negligible difference in the decay constants and mixing matrix elements. A linear interpolation of Φ_{B_s} and M_{B_s} from $am_s = 0.0359 \to 0.0343$ leads to at most a percent-level change in these quantities, which is too small to resolve within our large statistical errors. We therefore conclude that it is sufficient to forgo the interpolation to $am_s = 0.0343$ in our current analysis.

Although the strange-quark mass is integrated out in SU(2) HMχPT, the value of the strange valence-quark mass enters the chiral extrapolation described in Sec. V

via the linear fit in the heavy mass region that is constrained to unity in the limit $m_l \to m_s$. Once the slope in the linear region has been determined from fits to numerical lattice data, we estimate the errors in f_{B_s}/f_{B_d} and ξ due to the uncertainty in m_s by fixing the slope to this value and varying m_s within its stated uncertainty σ_{m_s} given in Eq. (83). This shifts the location of the SU(3) limit and hence the linear portion of the extrapolation in the horizontal direction by an amount $\pm\sigma_{m_s}$; consequently it shifts the location of the point at which we match onto SU(2) HMχPT in the vertical direction by the slope times $\pm\sigma_{m_s}$. From this method, we find that the systematic error in f_{B_s}/f_{B_d} due to the uncertainty in the valence strange-quark mass determination is 0.4% regardless of the smearing used for the heavy quark and the systematic error in ξ is 0.4% (0.3%) for the APE (HYP) data.

The value of the strange sea-quark mass does not explicitly enter the chiral extrapolation formulas. Nevertheless, it implicitly affects the determinations of f_{B_s}/f_{B_d} and ξ through the values of the SU(2) HMχPT low-energy constants. The latest results of the RBC and UKQCD Collaborations for f_π, f_K, and B_K [79] rely on reweighting [80] to self-consistently tune the strange sea-quark mass to its physical value during the chiral extrapolation of the pseudoscalar meson masses and decay constants. We can therefore estimate the effect of the incorrect strange sea-quark mass on f_{B_s}/f_{B_d} and ξ based on observations in the light pseudoscalar meson sector. Preliminary studies by RBC and UKQCD find that reweighting to the physical strange sea-quark mass leads to no statistically significant change in m_π and a 2% change in f_π [81]. If we assume that the unphysical strange sea-quark mass leads to a 2% error in the decay constants and matrix elements, then it will lead to a $2\% \times (\tilde{m}_s - \tilde{m}_d)/\Lambda_{\mathrm{QCD}} \sim 0.4\%$ error in the SU(3)-breaking ratios f_{B_s}/f_{B_d} and ξ.

In order to obtain the total systematic error in f_{B_s}/f_{B_d} and ξ due to the light- and strange-quark masses, we add the three estimates for the light-quark error, the strange valence-quark error, and the strange sea-quark error in quadrature. This leads to an error in f_{B_s}/f_{B_d} of 0.6% for both the APE and HYP data and an error in ξ of 0.6% (0.5%) for the APE (HYP) data.

G. Finite-volume errors

We estimate the uncertainties in the ratios f_{B_s}/f_{B_d} and ξ due to finite volume effects using one-loop finite-volume HMχPT. The effect of the finite spatial lattice volume is simply to turn the one-loop integrals that appear in the HMχPT expressions into sums, which we show in Eqs. (D13) and (D14). It is therefore straightforward to compute the corrections to our data given the parameters of our simulations. We find that the one-loop finite-volume corrections are about 1% at our lightest quark mass and even less at heavier masses. We therefore take 1% to be the

systematic uncertainty in f_{B_s}/f_{B_d} and ξ due to the finite spatial lattice volume.

H. $1/m_b$ corrections

Because we work in the static heavy-quark limit, our results for f_{B_s}/f_{B_d} and ξ neglect relativistic effects due to the finite b-quark mass. We therefore estimate the size of the omitted relativistic corrections using power-counting. The leading $1/m_b$ corrections to the decay constants and matrix elements are of $\mathcal{O}(\Lambda_{\mathrm{QCD}}/m_b)$. Because we are only computing the SU(3)-breaking ratios f_{B_s}/f_{B_d} and ξ, however, relativistic effects in these quantities are further suppressed by a factor of $(m_s - m_d)/\Lambda_{\mathrm{QCD}}$. Therefore, we expect the relativistic corrections to these quantities to be approximately

$$\frac{\Lambda_{\mathrm{QCD}}}{m_b} \times \frac{m_s - m_d}{\Lambda_{\mathrm{QCD}}} \sim 2\%, \qquad (84)$$

where the scale Λ_{QCD} cancels in the ratio, and we use the average $\overline{\mathrm{MS}}$ quark masses listed in the PDG [6].

VII. RESULTS AND CONCLUSIONS

Using the experimentally measured ratio of masses $m_{B_s^0}/m_{B_d^0} = 5366.6/5279.5 = 1.0165$ [6], we obtain the following values for the SU(3)-breaking ratios of B-meson decay constants and mixing matrix elements:

$$\frac{f_{B_s}}{f_{B_d}} = \begin{cases} 1.16(09)(10) & \mathrm{APE} \\ 1.14(05)(10) & \mathrm{HYP} \end{cases} \text{ and }$$

$$\xi = \begin{cases} 1.13(07)(10) & \mathrm{APE} \\ 1.13(05)(10) & \mathrm{HYP} \end{cases}, \qquad (85)$$

where the first errors are statistical and the second are the sum of the individual systematic errors added in quadrature. We find good agreement between the different link smearings, indicating that, despite the use of a single lattice spacing, discretization errors are small in the ratios. We therefore average the APE and HYP determinations to obtain our final results. After adding the statistical and

systematic errors for each link smearing in quadrature, we compute the average assuming that the two determinations are 100% correlated using the method of Ref. [82]:

$$\frac{f_{B_s}}{f_{B_d}} = 1.15(12) \qquad (86)$$

$$\xi = 1.13(12), \qquad (87)$$

where the errors reflect the combined statistical and systematic uncertainties. Although we computed these quantities in the static b-quark limit, the inclusion of the neglected $1/m_b$ corrections (which we estimate to be about 2%) produces a negligible change in the total errors in Eqs. (86) and (87) given the size of our other uncertainties; thus our results can be directly compared to phenomenological determinations and other lattice QCD results using relativistic b-quarks. As shown in Fig. 9, our results agree with the published results of the HPQCD Collaboration ($\xi = 1.258 \pm 0.025_{\mathrm{stat}} \pm 0.021_{\mathrm{sys}}$) [14] and the preliminary results of the Fermilab Lattice and MILC Collaborations ($\xi = 1.205 \pm 0.037_{\mathrm{stat}} \pm 0.034_{\mathrm{sys}}$) [15].

Although our results have significantly larger errors than the other $N_f = 2 + 1$ flavor determinations, in this work we have demonstrated the viability of our lattice computation method. In particular, we have introduced the new approach of using SU(2) heavy-light meson chiral perturbation theory to extrapolate $N_f = 2 + 1$ lattice QCD results for B-meson quantities to the physical quark masses. The largest sources of error in our calculation are from statistics and the chiral extrapolation, and we expect to reduce the sizes of both in a future work that analyzes the 24^3 domain-wall ensembles with the same lattice spacing [34]. Some of the 24^3 ensembles contain almost 3 times as many configurations as we have analyzed in this work. Furthermore, the use of a larger spatial volume will allow us to simulate at lighter valence and sea quark masses. Once we have made these improvements, our results will provide a valuable cross check of these important inputs to the CKM unitarity triangle analysis and determination of the ratio of CKM matrix elements $|V_{td}|/|V_{ts}|$.
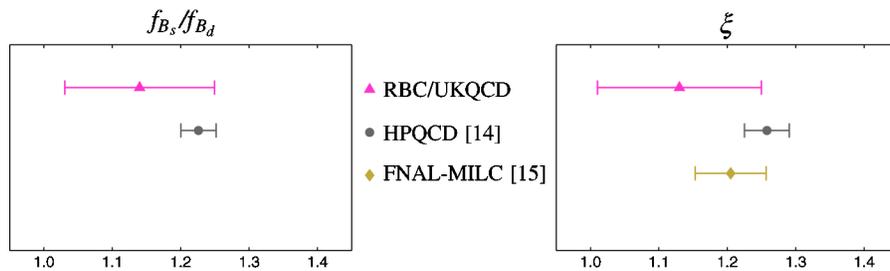

FIG. 9 (color online). Comparison of lattice QCD results for f_{B_s}/f_{B_d} and ξ. The magenta (triangle) denotes our new values obtained by averaging the APE and HYP results, the gray (circle) the values published by the HPQCD Collaboration [14] and the beige (diamond) the preliminary value presented by the FNAL-MILC Collaboration at Lattice 2009 [15].

APPENDIX A: SU(3) PROJECTION

In this appendix we describe the two SU(3) projection schemes used in this paper and show their equivalence in the weak coupling limit. Necessary properties of the projector mapping an arbitrary, complex 3×3 matrix on the SU(3) subgroup are idempotence and gauge-covariance. These properties are not sufficient to specify a unique projector and hence several choices exist. For APE smearing we use the unit circle projection [46] which is based on polar decomposition, while for HYP smearing we seek iteratively the matrix $U_{\max} \in SU(3)$ which maximizes $\mathrm{Re\,Tr}(U_{\max}V^{\dagger})$ [47].

First we describe the unit circle projection [46]. For a complex 3×3 matrix V with $\det(V) \neq 0$, we calculate the matrix

$$W = V[V^{\dagger}V]^{-1/2}, \tag{A1}$$

which is unitary by construction and has a spectrum lying on the unit circle. The square root is obtained by Jacobi matrix diagonalization. From W we obtain a special unitary matrix by computing

$$\bar{V} = [(\det(W))]^{-1/3}W. \tag{A2}$$

This projection is idempotent since an element of SU(3) is projected by Eqs. (A1) and (A2) back onto itself. The projection is also gauge covariant, as we now show. The

matrices V and $V^{\dagger}$ transform as

$$V \rightarrow G_L V G_R^{\dagger} \quad \mathrm{and} \quad V^{\dagger} \rightarrow G_R V^{\dagger} G_L^{\dagger}, \tag{A3}$$

and hence

$$V^{\dagger}V \rightarrow G_R V^{\dagger} V G_R^{\dagger}. \tag{A4}$$

Since $[V^{\dagger}V]^{-1/2}$ has the same transformation properties as $V^{\dagger}V$ one finds for the transformation of W

$$W \rightarrow G_L W G_R^{\dagger}, \tag{A5}$$

from which the gauge covariance of $\bar{V}$ follows.

Next we describe the projection method used for HYP smearing. This method is based on seeking a matrix $U_{\max}$ for which [47]

$$U_{\max} \in SU(3)|\mathrm{Re\,Tr}(U_{\max}V^{\dagger})\mathrm{is\ maximal}. \tag{A6}$$

The maximizing matrix $U_{\max}$ is found iteratively by decomposing it into its SU(2) subgroups as outlined in Refs. [47,83]. Although, by the compactness of SU(3), a global maximum exists, it is not guaranteed that this iterative procedure converges to the true maximum. Furthermore, the matrix obtained by the iterative procedure depends on the details of the iteration algorithm. In practice, however, one finds that $U_{\max}$ is numerically very close to $\bar{V}$, the SU(3) projection of the matrix V obtained from the unit circle projection [46] and hence the iteratively found maximum is close to the true maximum. Thus we choose

$$\tilde{V} = U_{\max} \tag{A7}$$

as the SU(3) projection of the complex matrix V. This projection is idempotent because for $V \in SU(3)$, unitarity and the triangle inequality imply the bound $\mathrm{Re\,Tr}(\tilde{V}V^{\dagger}) \leq 3$ which is uniquely saturated by $\tilde{V} = V$. By construction this projection is also gauge covariant.

Finally, we show that although the two projection methods are generally not equivalent they differ only at second order. For this discussion we assume that the iterative method converges to the global maximum and that the unprojected matrix V is approximately unitary and unimodular (which is true in the weak coupling limit).

In order to compare the two projection schemes, we first write the polar decomposition of V as

$$V = e^{i\theta}\bar{V}H, \tag{A8}$$

where $\theta \in (-\pi/3, \pi/3)$, H is a Hermitian matrix with eigenvalues $\lambda_1, \lambda_2, \lambda_3 > 0$, and $\bar{V}$ is the SU(3)-projected matrix given by Eq. (A2). We then diagonalize $H = M\Lambda M^{\dagger}$ [$\Lambda = \mathrm{diag}(\lambda_1, \lambda_2, \lambda_3)$ and $M \in SU(3)$] and substitute Eq. (A8) into Eq. (A6). The resulting function to be maximized is

$$\mathrm{Re\,Tr}(e^{-i\theta}U'\Lambda) = \mathrm{Re}(e^{-i\theta}(\lambda_1 u'_{11} + \lambda_2 u'_{22} + \lambda_3 u'_{33})), \tag{A9}$$

where u'_{ij} is an element of $U' \equiv M^\dagger \bar{V}^\dagger U_{\max} M \in SU(3)$. If the maximization is carried out over U(3) rather than SU(3), we could choose $u'_{11} = u'_{22} = u'_{33} = e^{i\theta}$. This satisfies the bound $\mathrm{Re}\,\mathrm{Tr}(e^{-i\theta} U' \Lambda)$ derived from the triangle inequality. If we maximize over SU(3) and $\bar{V}$ is already an element of SU(3) then it follows $U' = \mathbb{1}$ and there exists a unique maximum for $\theta = 0$ such that $\tilde{V} = \bar{V}$.

For the generic case maximizing over SU(3), the constraint $\det(U') = 1$ forces a maximum at $U' \neq \mathbb{1}$, and hence $\tilde{V} \neq \bar{V}$. Nevertheless, when V is approximately unitary and unimodular we can write $\theta = \delta\theta$ with $|\delta\theta| \ll 1$. Then $\lambda_k = 1 + \delta\lambda_k$ and $|\delta\lambda_k| \ll 1$. From that follows $u'_{kk} = 1 + i\delta_k$ with $|\delta_k| \ll 1$ ($k = 1, 2, 3$), and we can work to first order in all "small" quantities. Although U' can in principle develop small, off-diagonal elements, the constraint $U' \in SU(3)$ always implies that $\delta_k \in \mathbb{R}$ and $\delta_1 + \delta_2 + \delta_3 = 0$. Therefore, we must maximize

$$\sum_{k=1}^{3} \mathrm{Re}(1 + \delta\lambda_k + i\delta_k - i\delta\theta), \qquad (A10)$$

subject to the constraint $\delta_1 + \delta_2 + \delta_3 = 0$. Because this is independent of $\delta\theta$, this is equivalent to the case $\theta = 0$ discussed above. Consequently, to first order $\tilde{V} = \bar{V}$. This explains why the two projection schemes lead to numerically close results as reported in [46].

APPENDIX B: CONTINUUM QCD TO HQET MATCHING AND HQET RUNNING

In Eqs. (31) and (32) we separated the matching coefficients of the operators into three contributions: the QCD to HQET matching factor at scale m_b, the HQET running from m_b to m_c, and the HQET running from m_c to μ. Here we collect the results for these factors and present them for general numbers of flavors N_f and colors N_c. The Casimir factors that appear in the expressions are

$$C_F = \frac{N_c^2 - 1}{2N_c}, \qquad C_A = N_c, \quad \text{and} \quad T_F = \frac{1}{2}. \quad (B1)$$

The one-loop QCD to HQET matching factor for the axial current operator renormalized in the $\overline{\mathrm{MS}}$ scheme with naive dimensional regularization is calculated in Refs. [30,38]

$$\tilde{C}_A(m_b) = 1 - 2C_F \frac{\alpha_s(m_b)}{4\pi} + \mathcal{O}(\alpha_s^2), \qquad (B2)$$

while the renormalization group (RG) evolution factors entering Eq. (31) are given by [48,49]

$$U_A^{(N_f)}(\mu', \mu) = \left(\frac{\alpha_s^{(N_f)}(\mu')}{\alpha_s^{(N_f)}(\mu)}\right)^{d_A^{(N_f)}}$$
$$\times \left(1 + J_A^{(N_f)} \frac{\alpha_s^{(N_f)}(\mu') - \alpha_s^{(N_f)}(\mu)}{4\pi}\right)$$
$$+ \mathcal{O}(\alpha_s^2). \qquad (B3)$$

The coefficients in the evolution factor are

$$d_A^{(N_f)} = \gamma_A^{(0)}/2\beta_0, \qquad (B4)$$

$$J_A^{(N_f)} = \gamma_A^{(1)}/2\beta_0 - \gamma_A^{(0)}\beta_1/2\beta_0^2, \qquad (B5)$$

with

$$\beta_0 = \tfrac{11}{3}C_A - \tfrac{4}{3}T_F N_f, \qquad (B6)$$

$$\beta_1 = \tfrac{34}{3}C_A^2 - 4C_F T_F N_f - \tfrac{20}{3}C_A T_F N_f, \qquad (B7)$$

and the one- and two-loop anomalous dimensions

$$\gamma_A^{(0)} = -3C_F, \qquad (B8)$$

$$\gamma_A^{(1)} = -16C_F\left(\frac{49}{96}C_A - \frac{5}{32}C_F - \frac{5}{24}T_F N_f\right.$$
$$\left. - \left(\frac{1}{4}C_A - C_F\right)\frac{\pi^2}{6}\right). \qquad (B9)$$

The one-loop QCD to HQET matching factors for the $\Delta B = 2$ four quark operator are calculated in Refs. [50,53]:

$$\tilde{Z}_1(m_b, m_b) = 1 - \frac{8N_c^2 + 9N_c - 15}{2N_c}\frac{\alpha_s(m_b)}{4\pi} + \mathcal{O}(\alpha_s^2),$$
$$(B10)$$

$$\tilde{Z}_2(m_b, m_b) = -2(N_c + 1)\frac{\alpha_s(m_b)}{4\pi} + \mathcal{O}(\alpha_s^2). \quad (B11)$$

The operators O_L and O_S mix under RG evolution [see Eq. (32)], such that the evolution factors for the matching coefficients can be written as a 2×2 matrix:

$$U_L^{(N_f)} = \begin{pmatrix} U_{11}^{(N_f)} & 0 \\ U_{21}^{(N_f)} & U_{22}^{(N_f)} \end{pmatrix}. \qquad (B12)$$

Note that the matrix element $U_{12}^{(N_f)}$ is zero to all-orders in perturbation theory due to the fact that heavy-quark spin symmetry prohibits mixing from O_S into O_L. Because $\tilde{Z}_2$ in Eq. (B11) has no tree-level contribution, the two-loop expression for $U_{11}^{(N_f)}$ and one-loop expressions for $U_{21}^{(N_f)}$ and $U_{22}^{(N_f)}$ are sufficient to determine the $\mathcal{O}(\alpha_s)$ matching coefficients. The matrix elements in Eq. (B12) are given in Refs. [51–53]:

$$U_{11}^{(N_f)}(\mu', \mu) = \left(\frac{\alpha_s^{(N_f)}(\mu')}{\alpha_s^{(N_f)}(\mu)}\right)^{d_1^{(N_f)}}$$
$$\times \left(1 + J_{11}^{(N_f)} \frac{\alpha_s^{(N_f)}(\mu') - \alpha_s^{(N_f)}(\mu)}{4\pi}\right)$$
$$+ \mathcal{O}(\alpha_s^2), \qquad (B13)$$

$$U_{21}^{(N_f)}(\mu', \mu) = -\frac{1}{4}\left(\left(\frac{\alpha_s^{(N_f)}(\mu')}{\alpha_s^{(N_f)}(\mu)}\right)^{d_1^{(N_f)}} - \left(\frac{\alpha_s^{(N_f)}(\mu')}{\alpha_s^{(N_f)}(\mu)}\right)^{d_2^{(N_f)}}\right)$$
$$+ \mathcal{O}(\alpha_s), \qquad (B14)$$

$$U_{22}^{(N_f)}(\mu', \mu) = \left(\frac{\alpha_s^{(N_f)}(\mu')}{\alpha_s^{(N_f)}(\mu)}\right)^{d_2^{(N_f)}} + \mathcal{O}(\alpha_s), \qquad (B15)$$

with the coefficients

$$d_i^{(N_f)} = \gamma_{ii}^{(0)}/2\beta_0, \qquad (B16)$$

$$J_{11}^{(N_f)} = \gamma_{11}^{(1)}/2\beta_0 - \gamma_{11}^{(0)}\beta_1/2\beta_0^2, \qquad (B17)$$

and the anomalous dimensions

$$\gamma^{(0)} = \begin{pmatrix} -6C_F & 0 \\ 1 + 1/N_c & -6C_F + 4(1 + 1/N_c) \end{pmatrix}, \qquad (B18)$$

$$\gamma_{11}^{(1)} = -\frac{N_c - 1}{12N_c}(127N_c^2 + 143N_c + 63 - 57/N_c$$
$$+ 8\pi^2(N_c^2 - 2N_c + 4/N_c) - N_f(28N_c + 44)). \qquad (B19)$$

APPENDIX C: FINDING MATRIX ELEMENTS FROM GREEN'S FUNCTIONS

In this appendix we provide a derivation of Eqs. (63) and (72) which give the relationship between the Euclidean space correlation functions which are the direct results of our simulations and the matrix elements between normalized Hilbert space states which we wish to determine. In this appendix, all quantities are written in lattice units. The derivation of Eq. (63) follows the standard steps of inserting a complete set of energy eigenstates into the Green's functions $\mathcal{C}^{\text{LW}}(t, t_0)$ and $\mathcal{C}^{\text{WW}}(t, t_0)$ which are defined in Eqs. (59) and (60) and appear in the numerator and denominator of Eq. (63):

$$\mathcal{C}^{\text{LW}}(t, t_0) = \sum_n \sum_{\vec{x} \in V} \langle 0|A_0^L(\vec{x}, 0)|n\rangle\langle n|A_0^W(0)^\dagger|0\rangle e^{-E_n(t-t_0)}$$
$$(C1)$$

$$\mathcal{C}^{\text{WW}}(t, t_0) = \sum_n |\langle n|A_0^W(0)^\dagger|0\rangle|^2 e^{-E_n(t-t_0)}, \qquad (C2)$$

where E_n is the energy of the state $|n\rangle$, a state with unit normalization. Because of the translational invariance of

either the wall source operator A_0^W or the sum of the local operator A_0^L over a temporal hyperplane, the intermediate state $|n\rangle$ must have zero momentum. There is then a single, finite-volume state, $|B_q(\vec{p} = 0)_V\rangle$, separated from the other excited states by a nonzero energy gap, which will dominate as the time separation $t - t_0$ becomes large. Thus, in the limit of large $t - t_0$, Eqs. (C1) and (C2) become

$$\mathcal{C}^{\text{LW}}(t, t_0) = L^3\langle 0|A_0^L(0)|B_q(\vec{p} = 0)_V\rangle$$
$$\times \langle B_q(\vec{p} = 0)_V|A_0^W(0)^\dagger|0\rangle e^{-m_{B_q}^*(t-t_0)} \qquad (C3)$$

$$\mathcal{C}^{\text{WW}}(t, t_0) = |\langle B_q(\vec{p} = 0)_V|A_0^W(0)^\dagger|0\rangle|^2 e^{-m_{B_q}^*(t-t_0)}, \qquad (C4)$$

where we have used translational symmetry to replace the sum over $\vec{x}$ in Eq. (C1) with the factor L^3.

Finally, Eq. (63) follows by taking the ratio of Eq. (C3) and the square root of Eq. (C4) to remove the unwanted factor $\langle 0|A_0^L(0)|B_q(\vec{p} = 0)\rangle$ and recognizing that in the limit of large volume the unit-normalized state $|B_q(\vec{p} = 0)_V\rangle$ in Eq. (C3) and the covariant, delta-function normalized state $|B_q(\vec{p} = 0)\rangle$ in Eq. (57) are related by

$$\sqrt{2m_{B_q}L^3}|B_q(\vec{p} = 0)_V\rangle \rightarrow |B_q(\vec{p} = 0)\rangle. \qquad (C5)$$

This discussion is standard and has been repeated here to provide a familiar background for the derivation of Eq. (72) where a new approach, special to the static approximation, is required. The complication in Eq. (72) arises because of the use of a box source which is not translationally invariant and which produces a superposition of B-meson states with various momenta. In the static limit, all of these states are degenerate since their energy no longer depends on their momenta. Thus, we cannot assume that the large time limit, $t_f \gg t \gg t_0$ will project onto a unique ground state. However, as is worked out below, we can use an additional symmetry of the static approximation to show that the normalization of the box source cancels between the numerator and denominator of Eq. (72) [57].

Fortunately, this large set of degenerate states resulting from the momentum independence of the energy of the heavy-light meson, can be distinguished by a new conservation law which becomes exact in the static limit: the local conservation of heavy-quark number. The absence of spatial derivatives in heavy-quark actions shown in Eqs. (12) and (16) implies that the total number of heavy quarks at each spatial site is separately conserved. This conservation law results from the invariance of the heavy-quark action under the phase rotation of the heavy-quark Grassmann variables:

$$h(\vec{x}) \rightarrow e^{i\theta(\vec{x})}h(\vec{x}) \qquad (C6)$$

$$\bar{h}(\vec{x}) \rightarrow e^{-i\theta(\vec{x})}\bar{h}(\vec{x}) \qquad (C7)$$

in which a different phase $\theta(\vec{x})$ can be used for each spatial

site $\vec{x}$. In the quantum mechanical Hilbert space this symmetry corresponds to a family of operators $N_h(\vec{x}) = \bar{h}(x)\gamma^0 h(\vec{x})$ which commute with the Hamiltonian (continuum theory) or the transfer matrix (lattice theory). Thus, when interpreting our Green's functions we can introduce a complete set of *B*-meson states $|\tilde{B}_q(\vec{x})\rangle$ which are eigenstates of both the Hamiltonian and the number operators $N_h(\vec{x}')$ with a standard normalization:

$$N_h(\vec{x}')|\tilde{B}_q(\vec{x})\rangle = -\delta_{\vec{x},\vec{x}'}|\tilde{B}_q(\vec{x})\rangle \tag{C8}$$

$$\langle\tilde{B}_q(\vec{x})|\tilde{B}_q(\vec{x}')\rangle = \delta_{\vec{x},\vec{x}'}. \tag{C9}$$

Here the Kronecker delta, $\delta_{\vec{x},\vec{x}'}$, used above is appropriate for the discrete positions that appear in the lattice theory. The energy eigenstate $|\tilde{B}_q(\vec{x})\rangle$ can be thought of as composed of a static quark fixed to the position $\vec{x}$ together with a light-quark bound state centered at $\vec{x}$. The tilde notation is chosen to suggest the relation of these new states to our earlier energy and momentum eigenstates, $|B(\vec{p})_V\rangle$, which are standard superpositions of these $N_h(\vec{x})$ eigenstates:

$$|B_q(\vec{p})_V\rangle = \sum_{x\in V}\frac{e^{-i\vec{p}\cdot\vec{x}}}{L^{3/2}}|\tilde{B}_q(\vec{x})\rangle. \tag{C10}$$

Using these $N_h(\vec{x})$ eigenstates and the conservation of $N_h(\vec{x}')$ for all $\vec{x}' \in V$ it is now straightforward to derive Eq. (72). Substituting a sum over the complete set of degenerate ground states $|\tilde{B}_q(\vec{x})\rangle$ into the correlation function $C^{BB}(t, t_0)$ which appears in the denominator of Eq. (72) and is defined in Eq. (67) we find:

$$C^{BB}(t, t_0) = \sum_{\vec{x}\in\Delta V}\left\{\langle 0|\bar{h}(\vec{x})\gamma_0\gamma_5\left(\sum_{\vec{y}\in\Delta V}q(\vec{y})\right)|\tilde{B}_q(\vec{x})\rangle\right.$$
$$\left.\cdot\langle\tilde{B}_q(\vec{x})|\left(\sum_{\vec{y}'\in\Delta V}\bar{q}(\vec{y}')\right)\gamma_0\gamma_5 h(\vec{x})|0\rangle\right\}e^{-m_{B^*}(t-t_0)}, \tag{C11}$$

where we have used the conservation of local heavy-quark number to keep only terms where all of the heavy quarks are located at the same spatial position $\vec{x}$.

Similarly, we can evaluate $C^B_{O_i}(t_f, t, t_0)$ which appears in the numerator of Eq. (72) and is defined in Eq. (69):

$$C^B_{O_i}(t_f, t, t_0) = \sum_{\vec{x}\in\Delta V}\left\{\langle 0|\left(\sum_{\vec{y}\in\Delta V}\bar{q}(\vec{y}, t)\right)\gamma_0\gamma_5 h(\vec{x}, t)|\tilde{B}_q(\vec{x})\rangle\cdot\right.$$
$$\times\langle\tilde{B}_q(\vec{x})|O_i(\vec{x})|\tilde{B}_q(\vec{x})\rangle\cdot\langle\tilde{B}_q(\vec{x})|$$
$$\left.\times\left(\sum_{\vec{y}'\in\Delta V}\bar{q}(\vec{y}', t)\right)\gamma_0\gamma_5 h(\vec{x}, t)|0\rangle\right\}e^{-m_{B^*}(t_f-t_0)} \tag{C12}$$

$$= C^{BB}(t_f, t_0)\langle\tilde{B}_q(\vec{0})|O_i(\vec{0})|\tilde{B}_q(\vec{0})\rangle, \tag{C13}$$

where translational invariance of the matrix element

$\langle\tilde{B}_q(\vec{x})|O_i(\vec{x})|\tilde{B}_q(\vec{x})\rangle$ has been used to remove it from the sum over $\vec{x}$ causing that sum to assume the same form which appears in the box-box correlator $C^{BB}(t, t_0)$ given in Eq. (C11), after an application of charge conjugation symmetry. Equation (72) is then easily recognized from ratio of Eqs. (C12) and (C11):

$$M_{O_i} = \frac{1}{m_{B_q}}\langle\bar{B}_q(\vec{p}=0)|O_i(\vec{0})|B_q(\vec{p}=0)\rangle \tag{C14}$$

$$= 2L^3\langle\bar{B}_q(\vec{p}=0)_V|O_i(\vec{0})|B_q(\vec{p}=0)_V\rangle \tag{C15}$$

$$= 2\langle\tilde{\bar{B}}_q(\vec{0})|O_i(\vec{0})|\tilde{B}_q(\vec{0})\rangle \tag{C16}$$

$$= 2\frac{C^B_{O_i}(t_f, t, t_0)}{C^{BB}(t_f, t_0)} \tag{C17}$$

$$= 2\frac{C^B_{O_i}(t_f, t, t_0)e^{m^*_{B_q}(t_f-t_0)/2}}{\sqrt{C^{BB}(t_f, t)C^{BB}(t, t_0)}} \tag{C18}$$

where Eq. (C5), relating our two normalization conventions for momentum eigenstates, has been used to obtain the second equation.

This use of localized sources while making the static approximation may become more important as larger spatial volumes are used and the overlap between the translationally invariant wall sources and the physical states of interest becomes smaller. Of course, this same method can be used for localized sources with different spatial distributions such as Gaussian or atomic wave functions.

APPENDIX D: CHIRAL PERTURBATION THEORY FOR DECAY CONSTANTS AND MIXING PARAMETERS

In this section we present the NLO HMχPT expressions needed to extrapolate $N_f = 2 + 1$ domain-wall lattice data for heavy-light meson decay constants and mixing parameters to the physical quark masses and the continuum. Although we label the formulas with the subscript "*B*," we note that these functions can also be used to extrapolate *D*-meson decay constants and mixing matrix elements with the caveat that the low-energy constants (except for the light-light meson tree-level parameters f and B) are different for the case of *B*-mesons and *D*-mesons. We first show the SU(3) HMχPT formulas in Sec. D 1; we then take the appropriate limits of the SU(3) expressions to obtain those in SU(2) HMχPT in Sec. D 2.

1. SU(3) HMχPT expressions

The tree-level mass-squared of a meson composed of two domain-wall valence quarks with flavors *x* and *y* is

$$m^2_{xy} = B(m_x + m_y + 2m_{\text{res}}), \tag{D1}$$

where B is a continuum low-energy constant and m_{res} is the residual quark mass.

The NLO result for $\Phi_{B_x} = f_{B_x}\sqrt{m_{B_x}}$ in the partially-quenched domain-wall theory with $2+1$ flavors of sea quarks is [84,85]

$$
\Phi_{B_x} = \phi_0 \bigg\{ 1 - \frac{1}{16\pi^2 f^2} \frac{1 + 3g_{B^*B\pi}^2}{2} \sum_{f=l,l,h} \ell(m_{xf}^2) + \frac{1}{16\pi^2 f^2} \frac{1 + 3g_{B^*B\pi}^2}{6}
$$
$$
\times \bigg[R_X^{[2,2]}(\{M_X\};\{\mu\})\tilde{\ell}(m_X^2) - \sum_{j\in\{M_X\}} \frac{\partial}{\partial m_X^2}(R_j^{[2,2]}(\{M_X\};\{\mu\}))\ell(m_j^2) \bigg] + c_{\text{sea}}(2m_l + m_h) + c_{\text{val}}m_x + c_a a^2 \bigg\}, \quad \text{(D2)}
$$

where $f \approx 130.4$ MeV is the tree-level pion decay constant. The NLO expression for $M_{B_x} = 8/3 m_{B_x} f_{B_x}^2 B_{B_x}$ is similar [84,86]

$$
M_{B_x} = \beta_0 \bigg\{ 1 - \frac{1 + 3g_{B^*B\pi}^2}{16\pi^2 f^2} \sum_{f=l,l,h} \ell(m_{xf}^2) - \frac{1 - 3g_{B^*B\pi}^2}{16\pi^2 f^2} \ell(m_X^2) + \frac{1}{24\pi^2 f^2}
$$
$$
\times \bigg[R_X^{[2,2]}(\{M_X\};\{\mu\})\tilde{\ell}(m_X^2) - \sum_{j\in\{M_X\}} \frac{\partial}{\partial m_X^2}(R_j^{[2,2]}(\{M_X\};\{\mu\}))\ell(m_j^2) \bigg] + d_{\text{sea}}(2m_l + m_h) + d_{\text{val}}m_x + d_a a^2 \bigg\}. \quad \text{(D3)}
$$

In both the decay constant and the mixing matrix element, the only effect of the nonzero lattice spacing is a new analytic term proportional to a^2. These results agree with the continuum calculation of Sharpe and Zhang in the limit of three degenerate sea quarks [23]. We note that one is free to multiply the above expressions by arbitrary powers of the heavy-light meson mass m_{B_x} without modifying the chiral logarithms. This is because the chiral logarithm contributions to heavy-light meson masses are suppressed by $1/m_b$ and therefore of higher-order than we consider [87].

In the above expressions for Φ_{B_x} and M_{B_x}, the functions ℓ and $\tilde{\ell}$ are one-loop chiral logarithms:

$$
\ell(m^2) \equiv m^2 \ln\bigg(\frac{m^2}{\Lambda_\chi^2}\bigg), \quad \text{(D4)}
$$

$$
\tilde{\ell}(m^2) \equiv -\ln\bigg(\frac{m^2}{\Lambda_\chi^2}\bigg) - 1. \quad \text{(D5)}
$$

The function $R_j^{[n,k]}$ is due to single poles in the partially-quenched propagator:

$$
R_j^{[n,k]}(\{m\},\{\mu\}) \equiv \frac{\prod_{a=1}^k (\mu_a^2 - m_j^2)}{\prod_{i=1,i\neq j}^n (m_i^2 - m_j^2)} \quad \text{(D6)}
$$

and the sets of flavor-singlet masses that appear in the residue functions are

$$
\{\mu\} = \{m_L^2, m_H^2\}, \quad \text{(D7)}
$$

$$
\{M_X\} = \{m_X^2, m_\eta^2\}, \quad \text{(D8)}
$$

where m_X^2 is the mass-squared of a meson composed of two x valence quarks, $m_{L(H)}^2$ is the mass-squared of a meson composed of two $l(h)$ sea quarks, and $m_\eta^2 = (m_L^2 + 2m_H^2)/3$ for $2+1$ flavors of sea quarks.

For completeness, we also include the expressions for the decay constant and mixing matrix element at the unitary points. In the full QCD and isospin limits, the above expression for Φ_x becomes

$$
\Phi_{B_l} = \phi_0 \bigg\{ 1 - \frac{1}{16\pi^2 f^2}\bigg(\frac{1 + 3g_{B^*B\pi}^2}{2}\bigg)\bigg[\frac{3}{2}\ell(m_\pi^2) + \ell(m_K^2)
$$
$$
+ \frac{1}{6}\ell(m_\eta^2)\bigg] + c_{\text{sea}}(2m_l + m_h) + c_{\text{val}}m_l + c_a a^2 \bigg\}, \quad \text{(D9)}
$$

$$
\Phi_{B_h} = \phi_0 \bigg\{ 1 - \frac{1}{16\pi^2 f^2}\bigg(\frac{1 + 3g_{B^*B\pi}^2}{2}\bigg)\bigg[2\ell(m_K^2) + \frac{2}{3}\ell(m_\eta^2)\bigg]
$$
$$
+ c_{\text{sea}}(2m_l + m_h) + c_{\text{val}}m_h + c_a a^2 \bigg\}, \quad \text{(D10)}
$$

where $m_\pi^2 = m_L^2$ and $m_K^2 = (m_L^2 + m_H^2)/2$. Similarly, the expression for M_x becomes

$$
M_{B_l} = \beta_0 \bigg\{ 1 - \frac{1 + 3g_{B^*B\pi}^2}{16\pi^2 f^2}[2\ell(m_\pi^2) + \ell(m_K^2)]
$$
$$
- \frac{1 - 3g_{B^*B\pi}^2}{16\pi^2 f^2}\ell(m_\pi^2) + \frac{1}{48\pi^2 f^2}[3\ell(m_\pi^2) - \ell(m_\eta^2)]
$$
$$
+ d_{\text{sea}}(2m_l + m_h) + d_{\text{val}}m_l + d_a a^2 \bigg\}, \quad \text{(D11)}
$$

$$
M_{B_h} = \beta_0 \bigg\{ 1 - \frac{1 + 3g_{B^*B\pi}^2}{16\pi^2 f^2}[2\ell(m_K^2) + \ell(m_S^2)]
$$
$$
- \frac{1 - 3g_{B^*B\pi}^2}{16\pi^2 f^2}\ell(m_S^2) + \frac{1}{24\pi^2 f^2}[3\ell(m_S^2) - 2\ell(m_\eta^2)]
$$
$$
+ d_{\text{sea}}(2m_l + m_h) + d_{\text{val}}m_h + d_a a^2 \bigg\}. \quad \text{(D12)}
$$

The expressions for Φ_l and Φ_h agree with those derived by Goity in Ref. [88].

One can account for lattice finite volume effects at NLO in χPT by turning the one-loop integrals to sums. This yields an additive correction to the chiral logarithms [89]:

$$\ell(m^2) = m^2\left(\ln\frac{m^2}{\Lambda_\chi^2} + \delta_1^{FV}(mL)\right),$$
$$\delta_1^{FV}(mL) = \frac{4}{mL}\sum_{\vec{r}\neq 0}\frac{K_1(|\vec{r}|mL)}{|\vec{r}|}, \tag{D13}$$

$$\tilde{\ell}(m^2) = -\left(\ln\frac{m^2}{\Lambda_\chi^2} + 1\right) + \delta_3^{FV}(mL),$$
$$\delta_3^{FV}(mL) = 2\sum_{\vec{r}\neq 0}K_0(|\vec{r}|mL), \tag{D14}$$

where $\delta_i^{FV}(mL)$ is the finite volume correction to the infinite volume result and K_0 and K_1 are modified Bessel functions of imaginary argument.

2. SU(2) HMχPT expressions

The NLO SU(2) HMχPT expressions can easily be obtained from the SU(3) results in the previous subsection by integrating out the strange valence and sea quarks. After this procedure, however, the expressions for the decay constant and mixing matrix element differ for B_d-type mesons and B_s-type mesons.

First we consider B_d-type mesons composed of a b-quark and a light valence quark with mass m_x. In this case, we take the limits of Eqs. (D2) and (D3) assuming

$$\frac{m_x}{m_h}, \frac{m_l}{m_h} \ll 1. \tag{D15}$$

The resulting expression for Φ_{B_x} at NLO in the partially quenched domain-wall theory with two degenerate light sea quarks is

$$\Phi_{B_x} = \phi_0^{(2)}\left\{1 - \frac{1 + 3(g_{B^*B\pi}^{(2)})^2}{(4\pi f^{(2)})^2}\ell(m_{xl}^2)\right.$$
$$+ \frac{1 + 3(g_{B^*B\pi}^{(2)})^2}{(4\pi f^{(2)})^2}\left(\frac{1}{4}\right)[(m_L^2 - m_X^2)\tilde{\ell}(m_X^2) + \ell(m_X^2)]$$
$$\left. + c_{\rm sea}^{(2)}m_l + c_{\rm val}^{(2)}m_x + c_a^{(2)}a^2\right\}, \tag{D16}$$

where we use the superscript "(2)" to distinguish the

SU(2) low-energy constants from their SU(3) analogs in the previous section. The NLO expression for M_{B_x} is similar:

$$M_{B_x} = \beta_0^{(2)}\left\{1 - \frac{1 + 3(g_{B^*B\pi}^{(2)})^2}{(4\pi f^{(2)})^2}2\ell(m_{xl}^2)\right.$$
$$- \frac{1 - 3(g_{B^*B\pi}^{(2)})^2}{(4\pi f^{(2)})^2}\ell(m_X^2)$$
$$+ \frac{1}{(4\pi f^{(2)})^2}[(m_L^2 - m_X^2)\tilde{\ell}(m_X^2) + \ell(m_X^2)]$$
$$\left. + d_{\rm sea}^{(2)}m_l + d_{\rm val}^{(2)}m_x + d_a^{(2)}a^2\right\}. \tag{D17}$$

These results agree with the continuum partially-quenched calculation of Sharpe and Zhang in the limit $a \to 0$ [23]. The unitary QCD expressions can easily be obtained by the replacement $m_x \to m_l$. In the SU(2) theory, the effects of the dynamical strange quark are fully contained in the values of the low-energy constants, e.g. $\phi_0^{(2)}(m_h)$. For simplicity of notation, however, we suppress the functional dependence of the coefficients on m_h.

Next we consider B_s-type mesons composed of a b-quark and a heavy valence quark with mass m_y. Because the SU(2) chiral effective Lagrangian includes only two light quark flavors, this requires an extension of SU(2) χPT to the kaon sector, and the resulting theory is sometimes called kaon SU(2) chiral perturbation theory (KχPT) [34,90]. In this case, we take the limits of Eqs. (D2) and (D3) assuming

$$\frac{m_l}{m_y}, \frac{m_l}{m_h} \ll 1. \tag{D18}$$

The resulting NLO expressions for Φ_{B_y} and M_{B_y} are

$$\Phi_{B_y} = \phi_0^{(s)}\{1 + c_{\rm sea}^{(s)}m_l + c_a^{(s)}a^2\}, \tag{D19}$$

$$M_{B_y} = \beta_0^{(s)}\{1 + d_{\rm sea}^{(s)}m_l + d_a^{(s)}a^2\}, \tag{D20}$$

where we use the superscript "(s)" to distinguish the coefficients from those in Eqs. (D16) and (D17). Because the valence quark has been integrated out, there are no longer any chiral logarithms. The effects of both the valence and sea strange quarks are encapsulated in the values of the low-energy constants, e.g. $\phi_0^{(s)}(m_y, m_h)$.

[1] N. Cabibbo, Phys. Rev. Lett. **10**, 531 (1963).
[2] M. Kobayashi and T. Maskawa, Prog. Theor. Phys. **49**, 652 (1973).
[3] A. J. Buras, M. Jamin, and P. H. Weisz, Nucl. Phys. **B347**, 491 (1990).
[4] G. Buchalla, A. J. Buras, and M. E. Lautenbacher, Rev. Mod. Phys. **68**, 1125 (1996).
[5] T. Inami and C. S. Lim, Prog. Theor. Phys. **65**, 297 (1981);

65, 1772 (1981).

[6] C. Amsler *et al.* (Particle Data Group), Phys. Lett. B **667**, 1 (2008).

[7] V. M. Abazov *et al.* (D0), Phys. Rev. Lett. **97**, 021802 (2006).

[8] A. Abulencia *et al.* (CDF), Phys. Rev. Lett. **97**, 062003 (2006).

[9] A. Abulencia *et al.* (CDF), Phys. Rev. Lett. **97**, 242003 (2006).

[10] C. W. Bernard, T. Blum, and A. Soni, Phys. Rev. D **58**, 014501 (1998).

[11] J. Charles *et al.* (CKMfitter Group), URL http://ckmfitter.-in2p3.fr/.

[12] M. Bona *et al.* (UTfit Collaboration), URL http://utfit.roma1.infn.it/.

[13] E. Lunghi and A. Soni, Phys. Lett. B **666**, 162 (2008).

[14] E. Gamiz, C. T. H. Davies, G. P. Lepage, J. Shigemitsu, and M. Wingate (HPQCD), Phys. Rev. D **80**, 014503 (2009).

[15] R. T. Evans, E. Gamiz, A. El-Khadra, and A. Kronfeld (Fermilab Lattice and MILC), Proc. Sci. LATTICE2009 (2009) 245 [arXiv:0911.5432].

[16] G. P. Lepage, L. Magnea, C. Nakhleh, U. Magnea, and K. Hornbostel, Phys. Rev. D **46**, 4052 (1992).

[17] A. X. El-Khadra, A. S. Kronfeld, and P. B. Mackenzie, Phys. Rev. D **55**, 3933 (1997).

[18] C. W. Bernard *et al.*, Phys. Rev. D **64**, 054506 (2001).

[19] C. Allton *et al.* (RBC and UKQCD), Phys. Rev. D **76**, 014504 (2007).

[20] D. B. Kaplan, Phys. Lett. B **288**, 342 (1992).

[21] Y. Shamir, Nucl. Phys. **B406**, 90 (1993).

[22] V. Furman and Y. Shamir, Nucl. Phys. **B439**, 54 (1995).

[23] S. R. Sharpe and Y. Zhang, Phys. Rev. D **53**, 5125 (1996).

[24] C. Bernard, J. Laiho, and R. S. Van de Water (private communication).

[25] M. Della Morte, A. Shindler, and R. Sommer (ALPHA), J. High Energy Phys. 08 (2005) 051.

[26] M. Della Morte *et al.* (ALPHA), Phys. Lett. B **581**, 93 (2004).

[27] M. Albanese *et al.* (APE), Phys. Lett. B **192**, 163 (1987).

[28] M. Falcioni, M. L. Paciello, G. Parisi, and B. Taglienti, Nucl. Phys. **B251**, 624 (1985).

[29] A. Hasenfratz and F. Knechtli, Phys. Rev. D **64**, 034504 (2001).

[30] E. Eichten and B. Hill, Phys. Lett. B **234**, 511 (1990).

[31] D. Becirevic and J. Reyes, Nucl. Phys. B, Proc. Suppl. **129**, 435 (2004).

[32] O. Loktik and T. Izubuchi, Phys. Rev. D **75**, 034504 (2007).

[33] V. Gadiyak and O. Loktik, Phys. Rev. D **72**, 114504 (2005).

[34] C. Allton *et al.* (RBC-UKQCD), Phys. Rev. D **78**, 114509 (2008).

[35] S. Aoki *et al.* (PACS-CS), Phys. Rev. D **79**, 034503 (2009).

[36] D. Kadoh *et al.* (PACS-CS) Proc. Sci. LATTICE2008 (2008) 092.

[37] A. Bazavov *et al.* (MILC), Proc. Sci., LAT2009 (2009) 077.

[38] T. Ishikawa, Y. Aoki, T. T. Dumitrescu, J. M. Flynn, T. Izubuchi, and O. Loktik (to be published).

[39] Y. Iwasaki, Report No. UTHEP-118, 1983.

[40] A. Ali Khan *et al.* (*CP*-PACS), Phys. Rev. D **63**, 114504 (2001).

[41] Y. Aoki *et al.*, Phys. Rev. D **69**, 074504 (2004).

[42] K. G. Wilson, Phys. Rev. D **10**, 2445 (1974).

[43] D. J. Antonio *et al.* (RBC and UKQCD), Phys. Rev. D **77**, 014509 (2008).

[44] E. Eichten and B. Hill, Phys. Lett. B **240**, 193 (1990).

[45] W.-J. Lee, Phys. Rev. D **66**, 114504 (2002).

[46] W. Kamleh, D. B. Leinweber, and A. G. Williams, Phys. Rev. D **70**, 014502 (2004).

[47] G. S. Bali and K. Schilling, Phys. Rev. D **46**, 2636 (1992).

[48] X.-D. Ji and M. J. Musolf, Phys. Lett. B **257**, 409 (1991).

[49] D. J. Broadhurst and A. G. Grozin, Phys. Lett. B **267**, 105 (1991).

[50] J. M. Flynn, O. F. Hernandez, and B. R. Hill, Phys. Rev. D **43**, 3709 (1991).

[51] V. Gimenez, Nucl. Phys. **B401**, 116 (1993).

[52] M. Ciuchini, E. Franco, and V. Gimenez, Phys. Lett. B **388**, 167 (1996).

[53] G. Buchalla, Phys. Lett. B **395**, 364 (1997).

[54] K. G. Chetyrkin, Phys. Lett. B **404**, 161 (1997).

[55] J. A. M. Vermaseren, S. A. Larin, and T. van Ritbergen, Phys. Lett. B **405**, 327 (1997).

[56] K. I. Ishikawa, T. Onogi, and N. Yamada, Phys. Rev. D **60**, 034501 (1999).

[57] N. H. Christ, T. T. Dumitrescu, O. Loktik, and T. Izubuchi (RBC and UKQCD), Proc. Sci., LAT2007 (2007) 351.

[58] S. Aoki, T. Izubuchi, Y. Kuramashi, and Y. Taniguchi, Phys. Rev. D **67**, 094502 (2003).

[59] G. P. Lepage and P. B. Mackenzie, Phys. Rev. D **48**, 2250 (1993).

[60] S. Aoki and Y. Kuramashi, Phys. Rev. D **68**, 034507 (2003).

[61] U. Wolff (ALPHA), Comput. Phys. Commun. **156**, 143 (2004).

[62] A. S. Kronfeld and S. M. Ryan, Phys. Lett. B **543**, 59 (2002).

[63] D. Becirevic, S. Fajfer, S. Prelovsek, and J. Zupan, Phys. Lett. B **563**, 150 (2003).

[64] P. Boucaud *et al.*, Nucl. Phys. **B721**, 175 (2005).

[65] H. Ohki, H. Matsufuru, and T. Onogi, Phys. Rev. D **77**, 094509 (2008).

[66] C. Aubin *et al.* (MILC), Phys. Rev. D **70**, 114501 (2004).

[67] J. Noaki *et al.* (JLQCD and TWQCD), Phys. Rev. Lett. **101**, 202004 (2008).

[68] D. Becirevic, B. Blossier, E. Chang, and B. Haas, Phys. Lett. B **679**, 231 (2009).

[69] R. Casalbuoni *et al.*, Phys. Rep. **281**, 145 (1997).

[70] D. Becirevic and B. Haas, arXiv:0903.2407.

[71] I. W. Stewart, Nucl. Phys. **B529**, 62 (1998).

[72] A. Anastassov *et al.* (CLEO), Phys. Rev. D **65**, 032003 (2002).

[73] M. C. Arnesen, B. Grinstein, I. Z. Rothstein, and I. W. Stewart, Phys. Rev. Lett. **95**, 071802 (2005).

[74] S. Fajfer and J. F. Kamenik, Phys. Rev. D **74**, 074023 (2006).

[75] J. A. Bailey *et al.* (Fermilab Lattice and MILC), Phys. Rev. D **79**, 054507 (2009).

[76] M. Della Morte *et al.* (ALPHA), J. High Energy Phys. 02 (2008) 078.

[77] O. Buchmuller and H. Flacher, Phys. Rev. D **73**, 073008 (2006).

[78] Y. Aoki and J. Wennekers (RBC and UKQCD), Proc. Sci., LAT2007 (2007) 345.

[79] C. Kelly, P. A. Boyle, and C. T. Sachrajda (RBC and UKQCD), Proc. Sci., LAT2009 (2009) 087.

[80] A. Hasenfratz, R. Hoffmann, and S. Schaefer, Phys. Rev. D **78**, 014515 (2008).

[81] R. Mawhinney (RBC and UKQCD), Proc. Sci., LAT2009 (2009) 081.

[82] M. Schmelling, Phys. Scr. **51**, 676 (1995).

[83] F. D. R. Bonnet, D. B. Leinweber, A. G. Williams, and J. M. Zanotti, Phys. Rev. D **65**, 114510 (2002).

[84] D. Arndt and C. J. D. Lin, Phys. Rev. D **70**, 014503 (2004).

[85] C. Aubin and C. Bernard, Phys. Rev. D **73**, 014515 (2006).

[86] W. Detmold and C. J. D. Lin, Phys. Rev. D **76**, 014501 (2007).

[87] E. E. Jenkins, Nucl. Phys. **B412**, 181 (1994).

[88] J. L. Goity, Phys. Rev. D **46**, 3929 (1992).

[89] C. Bernard (MILC), Phys. Rev. D **65**, 054031 (2002).

[90] A. Roessl, Nucl. Phys. **B555**, 507 (1999).